EFFECT OF MICROWAVE RADIATIONS ON ELECTRICAL, MECHANICAL AND THERMAL PROPERTIES OF POLY (VINYL ALCOHOL) NANO COMPOSITE FILMS

BY

HAFIZ MUHAMMAD AFZAL

A Thesis Presented to the
DEANSHIP OF GRADUATE STUDIES

KING FAHD UNIVERSITY OF PETROLEUM & MINERALS

DHAHRAN, SAUDI ARABIA

In Partial Fulfillment of the
Requirements for the Degree of

MASTER OF SCIENCE

In

CHEMICAL ENGINEERING

December, 2016

KING FAHD UNIVERSITY OF PETROLEUM & MINERALS

DHAHRAN- 31261, SAUDI ARABIA

DEANSHIP OF GRADUATE STUDIES

This thesis, written by **Hafiz Muhammad Afzal** under the direction his thesis advisor and approved by his thesis committee, has been presented and accepted by the Dean of Graduate Studies, in partial fulfillment of the requirements for the degree of **MASTER OF SCIENCE IN CHEMICAL ENGINEERING.**

Dr. Mamdouh Al-Harthi
(Advisor)

Dr. Mohammed S. Ba-Shammakh
Department Chairman

Dr. Abdulhadi Al-Juhani
(Member)

Dr. Salam A. Zummo
Dean of Graduate Studies

Dr. Isam Al-Jundi
(Member)

4/1/17
Date

Dr. Mohammad Mozahar Hossain
(Member)

Dr. Shaikh Abdur Razzak
(Member)

Dedication

Dedicated to my father (Muhammad Ashraf)

ACKNOWLEDGMENTS

In the name of Allah the most Merciful and Beneficent

First of all, I'd like to thank ALLAH almighty, the most merciful and compassionate, for his support, help and generosity.

Now, I would like to express my special appreciation and thanks to my advisor Professor Dr. Mamdouh Al Harthi, you have been a tremendous mentor for me. His continuous support, patience, motivation and immense knowledge tuned me a lot during my MS study and related research. His guidance helped me in all the time of research and writing of this thesis. Beside my advisor, I am thankful to my committee members, Dr. Abulhadi Al-Juhani, Dr. Isam Al-Jundi, Dr. Mohammad Mozahar Hossain and Dr. Shaikh Abdurrazzak for their insightful comments and encouragement.

I appreciate Mr. Sarath P. Unikrri for his help and support in preparing nanocomposite film and handling characterization equipment and tools.

Conclusively, I acknowledge my gratitude to KFUPM and Department of Chemical Engineering for facilitating me in my MS study and research. Last but not the least, I am thankful and owe everything to my family (especially my father) and friends who encouraged and helped me at every stage of my personal and academic life and longed to see this achievement come true.

TABLE OF CONTENTS

LIST OF TABLES

LIST OF FIGURES

LIST OF ABBREVIATIONS

PVA	:	Poly (vinyl alcohol)
CNTs	:	Carbon nanotubes
DSC	:	Differential Scanning Calorimetry
FTIR	:	Fourier transformed infrared spectroscopy
SEM	:	Scanning electron microscopy
TGA	:	Thermogravimetric analysis
XRD	:	X-ray diffraction
VNA	:	Vector network analyzer
EMI SE	:	Electromagnetic interference shielding effectiveness
E	:	Activation energy
k_o	:	Frequency factor

ABSTRACT

Full Name : Hafiz Muhammad Afzal

Thesis Title : EFFECT OF MICROWAVE RADIATIONS ON ELECTRICAL, MECHANICAL AND THERMAL PROPERTIES OF POLY (VINYL ALCOHOL) NANO COMPOSITE FILMS

Major Field : Chemical Engineering

Date of Degree : December 2016

Modification of polymer nanocomposite properties using radiations is gaining wide interest and acceptance by the researchers both in academia and industry. Laser, Electron beam, gamma, UV, X-rays, and microwave are the common radiations being used to alter the properties of the polymers. Comparing to the other types, microwave radiation is easier to use, cheaper, and safer technology.

Poly (vinyl alcohol) (PVA) is a polymer that has been received significant interest from researchers who are working with films and packaging materials. In our research groups, we have studied and reported different systems of PVA blends [1-15]. Significant improvement in the properties of PVA was reported by reinforcing it with CNT and graphene [7-14]. Among a number of different Nano fillers, Graphene and CNT have emerged as promising fillers for polymer composites in the last two decades. The main advantage of adding nano filler in the weak polymer matrix as poly (vinyl alcohol) is to

give extraordinary properties enhancement favourable for different applications. The development of PVA nano composites with graphene was an important aim of current applied research work for use in the electric field. As electrical and electronic devices are used everywhere in our life. Their usage has been increased remarkably and we cannot imagine our modern life without using these important instruments. However, the electromagnetic radiations emitted from these instruments overlap with one another leading to damage or malfunctioning of the adjacent equipment. Consequently, the need of reliable and effective electromagnetic interference (EMI) shielding materials is essential. Recently, polymer based conductive composites have been attracted a considerable amount of attention by researchers owing to their low cost, low density, durability, good mechanical properties and a wide range of applications. PVA being a water soluble polymer is well known for its biocompatibility and non-toxicity. In recent years, graphene has gone one step ahead among the other nano fillers due to its unique characteristics. Graphene combines the layered structure of clays with excellent mechanical, thermal and electrical properties of carbon nanotubes, which eventually provides unique functional properties for the final products.

In this applied research work, we exposed the prepared films to microwave radiation to investigate the effect of irradiation on electrical, mechanical, thermal and morphological properties. Poly (vinyl alcohol) / graphene nanocomposites were prepared using solution casting technique. Samples were subjected to microwave radiations for 5, 10 and 15 min at a constant power of 200 watts. The nanocomposites were characterized before and after irradiation by scanning electron microscopy (SEM), X-ray diffraction (XRD), Fourier transform infrared spectroscopy (FTIR), Raman spectroscopy, differential scanning

calorimetry (DSC) and thermogravimetric analysis (TGA). Reduction in crystallinity and thermal stability of PVA was observed with incorporation of graphene due to restricted dynamic movement of chains and synergistic instability respectively. Microwave irradiation for 5 min improved the crystallinity from 46% to 55% and thermal stability (activation energy increased from 122 kJ $mole^{-1}$ to 128 kJ $mole^{-1}$) of the nanocomposites. Further irradiation caused a decreased in the crystallinity as well as in the thermal stability due to degradation. Furthermore, the isothermal crystallization kinetics were studied by employing the well-known Avrami model. An increase in the crystallization rate was observed with graphene incorporation. The thermal degradation kinetics were also studied by the help of TGA analysis. All the nanocomposites followed n_{th} order reaction mechanism and no change in degradation was observed due to the addition of graphene or the microwave irradiation except the changes in the kinetic parameters such as activation energy (E) and frequency factor (k_o). Moreover, increase in electrical conductivity from 0.021 S/cm to 3.55 S/cm was observed in 1% and 10% graphene incorporation in PVA matrix respectively. Composites acquired percolation threshold at 5% graphene incorporation with 2.17 S/cm DC conductivity. Bueche model and Scarisbrick model were applied for the prediction of electrical conductivity and the close match was found between experimental and theoretical conductivity using Scarisbrick model at geometrical factor (C) value 0.1. Vector network analyzer (VNA) was engaged in measuring the electromagnetic inference shielding effectiveness (EMI SE). EMI SE found to increase along with an increase in graphene contents. Improvement in both electrical properties, electrical conductivity, and EMI SE, was achieved after microwave irradiation. The decrease in tensile properties was found with the incorporation of graphene especially at

higher percentage due to agglomeration. Moreover, at higher graphene percentage the thickness of filler enrich side increased in bi-layered films which result in decrease of tensile strength.

ملخص الرسالة

الاسم الكامل: حافظ محمد افضل

عنوان الرسالة: تأثير أشعة الميكروويف على الخواص الكهربائية والحرارية لحشوات البولي فينيل الكحول النانوية المستخدمة في الالكترونيات

التخصص: الهندسة الكيميائية

تاريخ الدرجة العلمية: تعديل البوليمر النانوي خصائص بإستخدام الإشعاعات تحظى بالاهتمام على نطاق واسع، والقبول من جانب الباحثين في الأوساط الأكاديمية والصناعة على حد سواء. الليزر، إلكترون شعاع، غاما، والأشعة فوق البنفسجية، والأشعة السينية، والموجات الدقيقة هي الإشعاعات الشائعة المستخدمة لتغيير الخصائص للبوليمرات. مقارنة بالأنواع الأخرى، إشعاع الميكروويف أسهل للاستخدام، أرخص وتعتبر تقنية أكثر أمنا. بولي الفينيل الكحول (PVA) هو البوليمر الذي تلقي اهتماما كبيرا من الباحثين الذين يعملون مع الأفلام ومواد التعبئة والتغليف. في وتم ذكر تحسين كبير في خصائص ال PVA [1-15]. مجموعات البحث لدينا، درسنا أنظمة مزج مختلفة من ال والجرافين [7-14]. بين عدد من مختلف الحشوات الصغيرة، CNT و ذلك عن طريق التعزيز بواسطة ال PVA قد برزت كحشوات واعدة لمركبات البوليمر في العقدين الأخيرين. والميزة الرئيسية لإضافة CNT الجرافين، و ال إعطاء تعزيز للخصائص بصورة استثنائية (PVA) حشوات النانو في مصفوفة البوليمر الضعيفة كبولي الفينيل الكحول المركبة على مستوى النانو مع الجرافين هدف هام لعمل البحوث التطبيقية PVA مؤاتية لتطبيقات مختلفة. تطوير ال الحالية لاستخدامها في المجال الكهربائي. بما أن استخدام الأجهزة الكهربائية والإلكترونية في كل مكان في حياتنا. قد زاد استخدامها بصورة لافتة للنظر، ولا يمكننا أن نتصور حياتنا المعاصرة دون استخدام هذه الأجهزة الهامة. ومع ذلك، الإشعاعات الكهرومغناطيسية المنبعثة من هذه الأجهزة تتداخل مع بعضها البعض مما يؤدي إلى ضرر أو أعطال بصورة موثوقة أمر (EMI) المعدات المجاورة. ونتيجة لذلك، الحاجة إلى مصدار تشويش والدروع الكهرومغناطيسية

ضروري. اجتذبت مؤخرا، مركبات البوليمر على الموصلة قدرا كبيرا من الاهتمام من قبل الباحثين نظراً لتكلفتها كونه PVA المنخفضة، وانخفاض الكثافة، والمتانة، وخصائص ميكانيكية جيدة ومجموعة واسعة من التطبيقات. ال بوليمر قابل للذوبان في الماء معروف جيدا لتوافقه مع الحياة و كونه غير سام. في السنوات الأخيرة، قد تقدم الجرافين خطوة واحدة بين الحشوات علة مستوى النانو الأخرى بسبب خصائصه الفريدة. الجرافين يجمع بين هيكل الطبقات من ، الذي يوفر في (CNT) الطين ذات الخصائص الميكانيكية والحرارية والكهربائية الممتازة للأنابيب النانوية الكربونية .نهاية المطاف الخصائص الفنية الفريدة للمنتجات النهائية

في هذا البحث التطبيقي، تعرض الأفلام المعدة للموجات الإشعاعية للتحقيق في تأثير الإشعاعات على الخصائص الكهربائية والميكانيكية، الحرارية والمورفولوجية. بولي الفينيل الكحول/مركب الجرافين على مستوى النانو أعدت باستخدام تقنية الصب المحلول. تعرضت العينات للإشعاعات لمدة 5، 10 و 15 دقيقة تحت قدرة ثابتة مقدارها 200 وات. تم توصيف المركبات على مستوى النانو قبل وبعد إستخدام الإشعاع بالمسح الضوئي المجهر الإلكتروني والتحليل (DSC) ، طيف رامان، و القياس التفاضلي(FTIR)، (XRD) ، حيود الأشعة السينية(SEM) مع إدماج الجرافين بسبب تقييد PVA لوحظ انخفاض في التبلور والثبات الحراري ل .(TGA) ثيرموجرافيميتريك حركة السلاسل وعدم الاستقرار التآزر على التوالي. إشعاع الميكروويف لمدة 5 دقائق تحسن التبلور من 46% إلى 55% و الاستقرار الحراري (زادت طاقة التنشيط من 122 كيلو جول مول-1 إلى 128 كيلو جول مول-1) بالنسبة للمركبات على مستوى النانو. زيادة التعريض للإشعاع تسببت بإنخفاض في التبلور، وكذلك كما هو الحال في الثبات الحراري نتيجة للتدهور. وعلاوة على ذلك، جرت دراسة حركية التبلورذو درجة الحرارة الثابتة باستخدام نموذج أفرامي المعروف. ولوحظ زيادة في معدل تبلور مع إدماج الجرافين. ودرست أيضا حركية التدهور الحراري بمساعدة بالنسة للتفاعل ولوحظ عدم وجود تغيير في التدهور n جميع المركبات على مستوى النانو اتبعت الرتبة .TGA تحليل (E) بسبب إضافة الجرافين أو إشعاع الموجات الدقيقة باستثناء التغييرات في معاملات الحركية مثل طاقة التنشيط إلى 3.55 S/cm وعلاوة على ذلك، حدثت زيادة في الموصلية الكهربائية من 0.0210.021 .(ko) وعامل التردد على التوالي. اكتسبت المركبات عتبة الترشيح PVA مع إدراج الجرافين بنسبة 1% و 10% في مصفوفة ال S/cm في الموصلية. وقد طبق نموذج بوش و سكاريسبريك للتنبؤ بالموصلية S/cm مع إدماج الجرافين بنسبة 5% مع 2.17 الكهربائية ووجد وإرتباط وثيق بين الموصلية التجريبية والنظرية باستخدام نموذج سكاريسبريك عند معامل هندسية

تم إيجاد .(EMI SE) قيمته 0.1. يقوم محلل شبكة الناقلات بالمشاركة لقياس فعالية التدريع الكهرومغناطيسي (C) تزيد جنبا إلى جنب مع زيادة في محتويات الجرافين. وتحققت زيادة في كل من الخصائص الكهربائية، EMI SE ، بعد إشعاع الموجات الدقيقة. تم العثور على انخفاض في خصائص الشد مع إدماج SE EMI الموصلية الكهربائية و الجرافين خاصة عند النسب المئوية العليا بسبب التكتل. وعلاوة على ذلك، عند النسب المئوية العليا للجرافين سمك الحشوة الجانبي زاد في الأفلام ثنائية الطبقات، مما يؤدي إلى انخفاض قوة الشد.

CHAPTER 1

INTRODUCTION AND OBJECTIVES

1.1. Introduction

During the past half century, usage of both thermoplastics and thermosets (crosslinked) in our daily life has been increased sufficiently. The main disadvantage of both thermoplastics and thermosets materials is non-biodegradability that causing environmental pollution. Therefore, the development of biodegradable polymers is necessary that are easily available from natural resources and can apply for many applications.

Depending upon the starting material there are three techniques used for the preparation of the nanocomposites. These techniques include solution casting, melt intercalation, and In-situ polymerization. In the solution casting technique those materials process which are easily soluble in any volatile solvent. This methodology gaining interest in nanocomposite film production because of uniform distribution of the filler, very nice flatness, and high optical purity. The basic prerequisites for this technique are;

- The solubility of polymer must be good in a volatile solvent.
- The solution must be stable with almost no solid contents and minimum viscosity.
- The film should be easy to release from casting support and homogeneous.

To achieve the above requirement different tricks such as co-solvent, additives, anti-sticking agents, etc. are used. In this technique first, we dissolve the polymer in a favorable solvent like water to prepare a clear solution. In the same time, a homogeneous dispersion is achieved for filler in the same solvent using ultra-sonication. Filler dispersion than transferred to an aforementioned

solution of polymer and stirring of the mixture continued till complete homogenization of the ingredients. Later on, nanocomposite solution subjected to degassing under vacuum to remove the trapped air bubbles (In vacuum oven at a specific temperature or at ambient temperature). A schematic diagram of solution casting technique for PVA/graphene composite is shown in Figure 1.

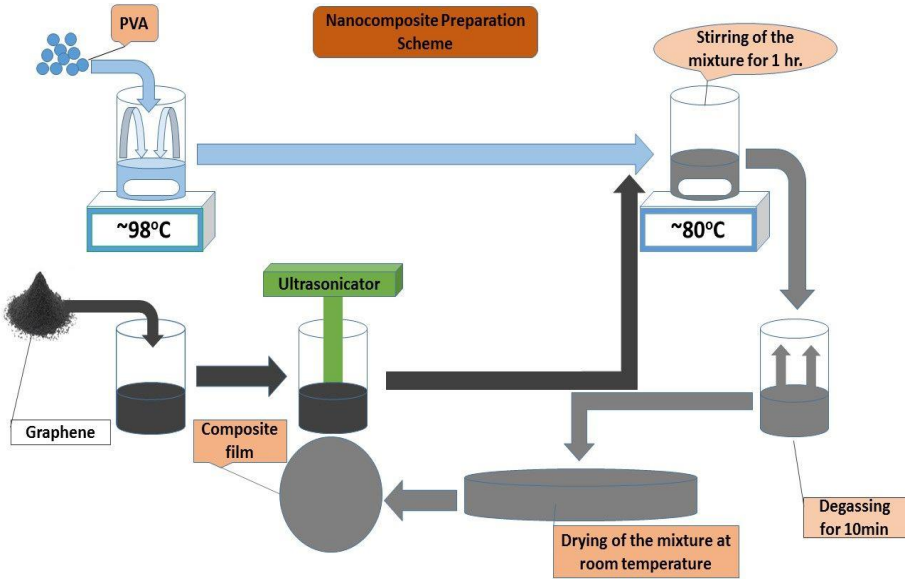

Figure 1: Solution casting technique for nanocomposite preparation.

Examples of the polymers and solvents used solution casting are Poly (vinyl alcohol) (PVA) / Gelatine/Starch / Methyl cellulose in water, Polycarbonates / Polyetherimide / Polyethersulfon in Methylene Chloride, Polyimides in dimethyl formaldehyde, Poly (vinyl chloride) in Methyl Ethyl-ketone or Tetrahydrofuran, Cellulose Di-acetate / Cellulose Tri-acetate in Methanol or Acetone, Cellulose Nitrate in Ester or Ether, et. [1], [2].

Poly (vinyl alcohol) (PVA) being a hydrophilic and biodegradable polymer has been used in innumerable applications. PVA as a 'green polymer' provides a unique opportunity for study comparative to the other organic polymers[3]–[6]. PVA nanocomposites with improved properties

such as an increase in percent crystallinity, thermal stability, electrical/thermal conductivity and mechanical strength have been reported[7]–[12]. In the nano-filler family, carbon containing nano fillers, such as graphene and carbon nanotubes (CNT's), have acquired huge attraction and interest among the researchers. These nano-fillers own remarkable properties like mechanical strength, thermal stability, electrical conductance and capability of chemical functionalization.[12] Graphene is in the spotlight in the nanotechnology field since 2004 because of its unprecedented properties.[13]–[15] Graphene incorporation with polymer matrix gives a combination of extraordinary thermal, mechanical and electrical properties compared to other materials[16]–[18]. Improved mechanical, electrical and thermal properties of PVA nanocomposite with graphene incorporation have been reported[19]–[21].

Thermal properties of the polymer are of great interest as mechanical properties and are susceptible to change by the incorporation of nano fillers. In thermal properties, such as the crystallization, degradation kinetics, melting point and temperature of crystallization are of particular interest. These thermal properties affect the mechanical and physical properties significantly [22]. Crystallization process controlled and monitored at a constant temperature state called as isothermal crystallization. The study of crystallization kinetics is very important as polymer are semi crystalline materials due to which crystal morphology, compare to crystallographic structure, controls the final properties of a polymeric product.[23] Moreover, crystallization kinetics is crucial for assessing the microstructural development. Isothermal crystallization kinetics can be described by Avrami model[22], [24]–[27]. Avrami model provides an opportunity to understand the crystallization process by taking, constant linear growth and constant nucleation rate, into consideration. Thermal stability of the composites is a basic factor to understand comprehensively their applicability in temperature environment. The thermal kinetic study provides the information

about the stability under different conditions and the degradation mechanism[28]–[30]. A perfect kinetic analysis demands the calculation of kinetic triplet (i) the kinetic model f (α), (ii) pre exponential fact k_o, and (iii) activation energy E. The kinetic model also referred as conversion function, is an algebraic expression describe the solid state reaction kinetics.[31], [32] Despite innumerable studies, the mechanism of degradation is still under investigation. Most of the investigation have accounted model free methods[33], [34] and model fitting technique for the non-isothermal degradation [35], [36].

Now a day's usage of electrical and electronic devices is everywhere and increasing continuously. Our lives without these instruments are not imaginable. However, these equipment emit different electromagnetic radiations which overlap with one another. It causes damage or malfunction in the adjacent equipment. In order to solve this problem, an effective EMI shielding is inevitable by using reliable materials. Electromagnetic interference shielding materials (EMI SE) are of great concern to prevent from these unwanted radiations emitted from surrounding equipment. Usually, metals are a candidate for EMI shielding due to electromagnetic radiations reflection from their electron rich surface. However, problems related to metals high density, flexibility, processing, and oxidation lower their preference as EMI SE. Thus the use of extrinsically conductive polymer nanocomposites gaining interest for EMI shielding due to easy processibility, light weight, environmentally stable and cost effectiveness [37], [38]. Many studies have been done to investigate the electromagnetic interference shielding of different polymers with graphene [5], [39]. The EMI SE of a nanocomposite depends on aspect ratio, intrinsic conductivity and dielectric constant of filler [40].

Recently, different conductive polymer nanocomposites attracted a considerable amount of attention for the researchers in this direction. Polymers are getting a great importance due to their

low density, corrosion resistance, low finishing cost, high range of toughness and ductility, durability and good mechanical properties. Polymers can be made electrically transporters by incorporation of different conductive fillers with varying size that can be used in wide range of applications [41]. Regarding electrical properties, polymers are divided into three groups; electrically conductor, semi–conductor and insulator. Electrically conducting polymers are further classified into three groups; intrinsically/inherently conducting polymers that have similar electrical, electronic and magnetic properties to that of metals and are commonly known as synthetic metals like polyacetylene, polyaniline, polypyrrole, polythiophene, poly (phenylene), poly (phenylene vinylene) and etc., extrinsically conducting polymers also known as conducting polymer composites, and ionically conducting polymers. Extrinsically conductive nanocomposites have gained a huge attraction of the researchers because of their applications in electronic and electrical appliances as sensors, electromagnetic interference shielding materials, capacitors, electrostatic discharge materials, etc. [42], [43]. In this study, we will concentrate our focus towards the third type of electrical conducting group. In which we will incorporate insulator polymer matrix with electrical conducting polymer like graphene. The dielectric constant, DC and AC electrical properties of pure polymer matrixes, as well as nanocomposites, have been studied in detail. The mechanism behind increase or decrease in mentioned electrical properties by incorporation of different nano-fillers thoroughly explained and understood [44]–[46]. Moreover, several reports have written on the investigation of nano-filler functionality to increase its compatibility with the polymer matrix, dielectric and electrical properties of polymer nanocomposites [47]–[50]. Poly (vinyl alcohol) (PVA) being a biodegradable and water soluble polymer gives a distinctive option for research compare to the other polymers[3]–[5]. Electrically conductive PVA nanocomposites with improved electromagnetic interference shielding (EMI) and

mechanical strength have been investigated [51], [52]. Prediction of DC conductivity using different theoretical models also is a hot topic among the researchers. There are many theoretical models like Voet, Scarisbrick, Bueche, McCullough, Lichtenecker equation, the Jayasundere-Smith equation, Maxwell–Sillars–Wagner, Kerner expression, Bruggeman model etc. successfully employed to predict polymer nanocomposites properties. These effective properties include AC, DC conductivities, dielectric constant, thermal conductivity, magnetic permeability, etc. In these theoretical predicting models they considered the shape of nano-filler like platelet, short fiber, particulate and continuous fiber. Structural parameters that cause sharp transition at percolation point also interpreted by these models. Modelling for electrical permittivity (dielectric constant) gave promising result between experimental and theoretical models [46], [53]–[59]. However, still, there is not any general model that is applicable for all nanocomposite systems. Therefore confirmation of these prevailing models is required to determine their validity and constraints. Scarisbrick, Bueche, and McCullough models are usually practiced for forecasting DC conductivity of polymeric nanocomposites [46].

Graphene has sp^2 hybridized monolayer structure with a two-dimensional arrangement of carbon atoms. Due to outstanding reinforcement, unique physical characteristics and electrical/mechanical properties graphene have acquired substantial interest among the researchers [13], [15] Graphene incorporation gives extraordinary electrical and mechanical properties to mother polymer matrix compared to other nano-fillers [16], [18]. Improvement in electrical, thermal and mechanical properties of PVA / graphene nanocomposites have been investigated [9], [51]. Thus, it is expected that graphene with high conductivity and large aspect ratio would give high EMI SE. In this applied research work to develop polymer composites with conductivity can be applied for a number of important technological applications like conductive coating, antistatic

materials, a chemical sensor, absorbing microwave, dye-sensitized, gas barrier and bipolar plates. The composite with the insulating-semiconducting surface can be used in electronics, aerospace, defense, and medical industry as EMI shielding materials for storing electronic components, and for protecting the environment from harmful radiation. The composite having resistivity of the upper surface in insulating zone and bottom surface in the antistatic zone can be used as electrostatic charge dissipation materials. The advantage of using these insulating-semiconducting materials is that the risk of getting an electrical shock is minimal because one surface is insulating in nature.

To achieve remarkable properties, we have to focus on the mechanism of properties' enhancement. From a basic understanding of dispersion and interfacial interactions of nano graphene with polymer matrix are key factors. So, the main challenge is to achieve nice dispersion and strong interfacial interaction. The strong interaction between graphene sheets makes them difficult to disperse homogeneously in the polymer matrix. Therefore, filler-polymer effective interaction and homogeneous dispersion are necessary to obtain promising results. As the demanding objective in the development of the nanocomposite is to attain fully dispersed and effective interaction of the filler with the polymer matrix. Therefore, many studies have been conducted on the functionalization of the nano-filler,[60], [61] small chain insinuation[62] and peroxide addition during melt-mixing.[63] The researcher are still trying to find out the green technique to acquire better interaction among the polymer matrix and nano-filler. Irradiation of polymer nano-composite is considered as a useful tool to improve the structural, thermal, electrical and mechanical properties by inducing crosslinking or degradation. The change in properties of a polymer under the effect of ionizing radiation depends on whether the polymer chains go to crosslinking or chain-scission. Radiation can cause both cross-linking and chain-scission,

depending upon the radiation power, chemical structure, crystallite size and the environment.[64] The degradation of PVA by irradiation has been studied by gamma rays.[65]–[67] Microwave radiations have high and rapid penetration power with a significant effect on the polar compounds. As microwave irradiation has proven to be the economical, fast and green technique for the preparation of polymer nano-composites. Studies have been made to scrutinize the role of microwave irradiation in graphene polymer interaction.[12], [68]–[72].

To the extent of our knowledge, so far no work has been conducted on microwave irradiation of PVA / graphene nanocomposites. Therefore, this study aims to investigate the effect of microwave irradiation on properties of PVA/graphene nanocomposites. The significance of this work was also due to the interest gained by the Polymer/graphene nanocomposites in daily life applications. Graphene incorporation with polymer matrix gives remarkably enhanced properties. These nanocomposites give promising results in applications such as electronics, aerospace, structural, medicine and environment. These unique properties are not available in other traditional nanocomposites. Graphene has been introduced as a storm in nanotechnology field from 2004. Its remarkable properties can convert it into a "magic bullet". Since 2000, approximately 30,000 research papers have been published on different methods. Almost $67 million graphene business has been reported by the BBC in 2015. It will boom up to $680 million until 2020. Similarly, graphene production volume will be increased to 573 tons by 2017 from 28 tons in 2010 [15].

1.2. Objectives

1. Development of conducting polymer nanocomposites based on PVA and graphene.
2. Characterization of polymer nanocomposites of PVA and graphene by studying electrical properties (DC conductivity and electromagnetic interference shielding effectiveness), thermal properties, mechanical properties and morphological (Crystallinity) changes.
3. Study the effect of microwave radiations on polymer composites of PVA with graphene.
4. Crystallization kinetics were conducted before and after the irritation using non-isothermal model. Investigation of the effect of microwave irradiation was done by re-characterizing irradiated samples through studying the electrical properties (DC conductivity and EMI SE), thermal properties, mechanical properties and morphological (Crystallinity) changes.
5. Study the mechanism of thermal degradation of un-irradiated and irradiated PVA composites.

CHAPTER 2

LITERATURE REVIEW

2.1. Poly (vinyl alcohol)

Polyvinyl Alcohol is considered as most likely water soluble material for many commercial applications. It is tasteless, odorless, biodegradable and biocompatible. As it is water soluble, it is slightly soluble in ethanol, but it is not soluble in other organic solvents. It is also readily blended with a number of natural materials and can exhibit properties that are compatible with a range of applications. This inclusion of natural fibers and fillers can give further improvements in mechanical properties without compromising overall degradability. Therefore, the potential benefits of PVA, given its water soluble characteristics, are huge, but this must be offset against practical considerations of its long term life cycle in changeable environmental conditions. Poly (vinyl alcohol) is having atactic stereoisomerism and partially crystalline. At a microstructure level, it contains 1,3-diol linkages with some percent 1,2-diols depending on the precursor (vinyl ester) polymerization condition. As of water soluble nature, its mechanical properties depend upon humidity. With the increase in humidity, the resultant material will be soft and tough while low humidity, produce hard and brittle material. Polyvinyl alcohol is an excellent emulsifier, having extraordinary film forming and adhesive properties. It has also resistive properties with non-polar solvents, grease, and oil. It has the capability to act as a barrier for aroma and oxygen and equipped with high flexibility and tensile strength. However, high tensile strength and flexibility are strongly effected by humid environment. In highly humid environment water get absorbed resultantly lower the tensile strength while increasing the tear strength and elongation. PVA starts melting at around 230 ^{o}C depending on the degree of hydrolysis because melting point decreases for partially

hydrolyzed up to about 190 °C. PVA is almost incompressible having Poisson's ratio from 0.42 to 0.48 [3].

2.1.1. Effect of different fillers on PVA

Crystallinity means how much order is there in the structure of a solid material. The crystallinity of a solid causes a big effect on its density, diffusion, and hardness. The degree of crystallinity of PVA / Starch blend having 4 g/4 g ratio does not change up to 3.78 g glycerol. By increasing the quantity of glycerol, the crystallinity decreases because of inhomogeneity. The increase in the exposure time of PVA / Starch blend to natural environment increases the crystallinity of PVA because of breakage of hydrogen bonding presence within the molecules, thus facilitating the decrease in amorphous structure of the polymers within the blends. Crystallinity increases by the addition of nano-TiO2 due to intermolecular hydrogen bonding between the –OH in PVA and nano-TiO2. The crystallinity of PVA also decreases with increase in starch contents while laser irradiation causes the removal of plasticizer and recovers the PVA crystallinity. The crystallinity of PVA also decreased with the incorporation of CNT and starch due to the bond formation in all three materials at the expense of present hydrogen bonding within PVA. The crystallinity of PVA also decreases in the presence of nano graphene with starch. [9]–[11], [21], [73]–[76]

Mechanical properties like tensile strength, dynamic modulus, and elongation film properties are strongly affected by the degree of polymerization. The tensile strength also increases with increase in the degree of hydrolysis. However, as well as these factors, the humidity also has a marked effect on physical properties. At low humidity, PVA film is hard and brittle, while at high humidity it is soft and flexible due to the plasticizing effect of the water vapor. This dependence is greater for partially hydrolyzed than those that are fully hydrolyzed. We can come up with modified

mechanical properties that enable the PVA to be used for many other applications with the addition of different fillers or by exposing PVA in different condition. Incorporation of nano fillers such as Nano clay, nano-SiO2 into polymers gives an increase in mechanical properties at the expense of a decrease in moisture absorption capability. Nano-TiO2 leads to increase in mechanical properties of PVA and starch blends such as modulus of elasticity and tensile strength. This increase in mechanical properties is because of adsorbed moisture on nano filler titanium dioxide surface. Tensile properties, the storage modulus of PVA also decreases with the incorporation of starch while laser irradiation recover by increasing heterogeneity. It was investigated that decrease in mechanical properties can be overcome by adding carbon nano-tubes. The increase in interaction between polymer's hydroxyl group and oxygenated groups in CNT cause tortuosity which lead to decrease the uptake of water and increase in homogeneity. Furthermore, graphene incorporation up to 0.5%wt increases the strength and Young's modulus without effecting the ductility of original PVA. Studies also have shown an increase in Young's modulus, yield stress, storage modulus and dynamic mechanical properties by the incorporation of graphene oxide with PVA [9]–[12], [21], [73]–[82].

The thermal properties of the polymer are of great interest as mechanical properties and can undergo change or modification with the addition of different filler. Among these thermal properties, heat of crystallization, the heat of degradation, melting point and temperature of crystallization are of particular interest. In the case of PVA/ Starch blend heat of crystallization, heat of melting and degree of crystallinity does not change at low concentration of glycerol incorporation. The crystallinity of aforementioned blend suffers drastically when glycerol incorporation increased from a specific value. Incorporation of glycerol in PVA / Starch blends also lower the thermal stability of the blend because of plasticization effect. Dilution occurs of the

glycerol effect with ageing and resultantly increases in heat of fusion, the heat of crystallization, the temperature of crystallization and melting point occur of the blend. Natural weather ageing, remove the glycerol contents and break the hydrogen bonding within starch and PVA. Ageing also increase the thermal stability of PVA by removing an amorphous portion. However, for the blend, thermal stability increases up-to a certain limit after that again a reduction in thermal stability starts.

Irradiation with laser gives an increase in thermal properties like melting point, crystallization temperature, the heat of crystallization, the heat of fusion and degree of crystallinity as a function of glycerol amount percent. The thermal analysis also investigated the increase in blend homogeneity, thermal stability and residual char with the incorporation of CNT. Thermal stability also increase with the addition of graphene in PVA / Starch blend because of hydrogen bonding in the nano graphene particles and polymer matrix[9]–[12], [21], [73]–[82]

2.2. Poly (vinyl alcohol) and Graphene Nanocomposites

Graphene has sp^2 hybridized monolayer with a two-dimensional arrangement of carbon atoms. It is the single layer having benzene ring like structure as a hexagonal lattice with a sheet having few atoms thickness (33 A^0) [13]. Graphene converts an insulator to conducting material even at significant lower %age loading. It has outstanding reinforcement, electrical and mechanical properties with unique physical characteristics. When it combines with the layered structure of clays then impart excellent mechanical, thermal and electrical properties, which ultimately gives unique functional properties to the final products. Since the isolation of single sheet of graphene by Novoselov et al. [14]graphene has been attracted the attention of researchers in making novel nanocomposites with the tremendous increase in mechanical properties like tensile strength,

Young's modulus, etc. [83]. In recent years, graphene gained tremendous progress and enormous interest on other nano fillers due to its unique characteristics and high surface area. Graphene is known to be mixed with graphene oxide for many different applications [84], [85]. The initial development of graphene oxide from graphite was via acid treatment (Hummer's Reaction) to exfoliate graphene sheets. This method is non-hazardous and less time consuming comparing to already employed methods [88]. Graphene has unique features which make it a high potential material for near future research.

The following studies are mainly focused on employing graphene based nano filler to poly (vinyl alcohol), Xu et al., [89]investigated that the preparation of PVA/graphene oxide nanocomposites. He found 92.2% higher tensile strength, ductile, strong with 167% higher modulus compared to the pure PVA polymer. Thermogravimetric analysis of TGA studies confirmed that the improved thermal stability. This improvement in mechanical and thermal properties was due to homogeneous dispersion and aligned graphene oxide sheets in the poly (vinyl alcohol) along with strong interfacial hydrogen bonding interaction between the components contributed to enhancement in the properties. Similarly, Zhao et al., [90] prepared a stable dispersion of GO in water with the help of Sodium Dodecyl Benzene Sulfonate (SDBS) by sonication. Then the composite was prepared by blending the stable graphene oxide solution with PVA powder. They observed remarkable enhancement observed in the thermal and mechanical properties; even at 1.8vol% graphene loading 150% improved tensile strength with 10 times high Young's modulus achieved. Liang et al., [83] have prepared PVA /graphene oxide nanocomposites by simple solution casting technique. They found effective reinforcement and molecular scale distribution of graphene oxide into the matrix of PVA. This gives an extraordinary increase in mechanical properties; that is to 0.7wt% GO 76 percent increase in tensile strength and 62 percent in modulus

of elasticity. Zhang et al., [91] prepared hydrogel of graphene and poly (vinyl alcohol) composites as a novel biomaterial by solution mixing and freeze-thaw technique. They could obtain 132% increase in tensile strength and 36% improved compressive strength by employing 0.8wt% GO as compared to the pure PVA hydrogels. The water resistance capability of PVA polymers is very vital while considering these nanocomposites for biomedical and packaging applications. Incorporation of GO at a specific level also do not affect the toxicity of poly (vinyl alcohol). A significant improvement in mechanical properties (212% higher tensile strength with 34% increase in ductility compare to virgin PVA) obtained at very low loading of graphene. They obtained 48.8%/-105.2% increase in water resistance property of PVA by the addition of 0.5wt% loading of graphene nano filler as investigated by Wang et al.,[5]. Huang et al., [92] prepared PVA-GO nano sheet composites by simple solution mixing process. TEM and XRD proved fully exfoliated, uniformly dispersed and oriented along the direction of the film surface. A dramatic change was observed in the barrier property, where the permeability of composite film decreased up to 98% for oxygen and 68% for water at a very small loading of 0.72 vol. % of graphene. This change was attributed to the strong interfacial adhesion due to hydrogen bonding between PVA and graphene nanocomposite. In a more sophisticated study**,** Cheng et al., [93] used PVA-grafted graphene oxide instead of pristine GO alone to further improve the PVA-nanocomposite properties. They achieved a very remarkable increase in mechanical properties as 88% and 150% respective increase in Young's modulus (modulus of elasticity) and tensile strength. Elongation at break increased 22% with 1 wt. % addition of filler compare to 15% with pristine GO. Means that g-GO made PVA not only stronger but also tough and this increase are due to good compatibility between g-GO/PVA as well as strong interfacial interaction. Wang et al., [94] (different group) reported the preparation of PVA/GO nanocomposites via electrospinning method and their characterization.

They realized 3D porous structure. The nanofibers obtained for their mechanical, thermal and morphological analysis. They observed a decrease in decomposition temperature about 38-50^{o}C while with the 42 times greater tensile strength even at a loading of 0.02 wt. % of GO in the PVA matrix. Lee et al., [95] have exclusively studied the change in crystallization behavior of PVA-graphene (disc-shaped) nanocomposites. At very low concentrations (0.5 wt %) it was found that graphene enhanced the crystallinity up to 18.8% of the polymer by acting as a nucleating agent. Disc-shaped nano graphene regulates the size of the crystal. In addition, it was also found that at higher concentration of graphene (>1 wt. %), the mechanical properties were found to increase with respect to graphene content. Latif et al., [96] prepared pectine/PVA/graphene composites and compared with the dielectric properties of hydrated and dry films of the composites. They investigated the effect of controlled hydration in the humidity chamber and found step impact on dielectric permittivity of the composite. Increased dielectric permittivity was mainly due to the chain-bound water complexes formation between pectine, PVA and graphene molecules contributing of polarizabilities from the dipole. It was found that dielectric permittivity increased than predicted by Maxwell Wagner rule of mixing. Ye et al., [97] studied the alkali PVA/graphene electrolyte. They observed significant improvements in ionic conductivity because of exfoliated and highly connected in the form of a channel. This composite also suppressed methanol crossover for PVA membrane reinforced with graphene for fuel cell application. An optimum loading of 0.7 % of graphene caused 126% enhancement in ionic conductivity and 55% reduction in methanol permeability. At high graphene loading 73% improvement in Young's modulus observed. All these factors eventually enhanced the cell performance by 148% increase in power density. Ma et al., [98] prepared nanocomposite films of PVA and glucose-reduced graphene oxide (rGO) by using solution blending method. The aqueous suspension stability of rGO increased by

incorporating poly (N-vinyl-2-pyrrolidone) (PVP) as a surfactant. The results revealed that the tensile strength and Young's modulus of nanocomposite film of poly (vinyl alcohol) contain 0.7 wt.% PVP-RGO were 105-154 MPa and 3.3-4.9 GPa respectively, which is 47% and 48% higher as compare to pristine graphene/PVA. Recently, Shang et al., [99] produced poly (vinyl alcohol)/graphene nanoribbon nanocomposites by using a solution mixing technique. Graphene nanoribbon was produced by carbon nanotubes using chemical approach oxidants. The prepared nanoribbon graphene interacted with PVA through hydrogen bonding and also contained a lot of oxygenated groups that provides homogeneous dispersion in water as well as in PVA. Nanocomposites showed considerable improvements in terms of mechanical performance as 85.7% increase in tensile strength with 65.2% increase in Young's modulus. Results also showed that increase thermal stability of PVA matrix due to enhancing interaction of nanoribbon graphene that means nanoribbon graphene is suitable for preparation of high performance nano-composites. Jose et al., [21] prepared polymer films of PVA/starch/graphene using glycerol as a plasticizer. A solution mixing and casting technique was employed for preparing the films. The results showed that a graphene loading of 0.5wt. % is an optimum loading in terms of best mechanical properties. Thermal studies of the composite also showed enhancement in thermal stability of nano-composite compare to PVA matrix. As stated above, many papers are published in the area of PVA films. However, electromagnetic interference shielding effectiveness EMI SE, thermal and electrical conductivity, dielectric constant, factor and their modelling for this system are not completely studied. The current proposal will be mainly focused on to investigate the electrical properties of poly (vinyl alcohol) and graphene system.

2.3. Effect of Irradiation on Nanocomposites

The basic mechanism of microwave radiated polymer is the reorientation in dipoles under the radiation. The effect of microwave on polymeric materials is dependent on the strength of dipole, its chemical structure, molecular weight and dipole state. The effect of microwave radiation is greater in the polymer when it is in a melt state, less in a rubber, and ignorable little effect on a glassy or crystalline polymer. As microwave has high and rapid penetration even heating abilities, thick films of polymer composites are considered ideal for applications of microwave radiation processing. Increase in adhesion and improvement in mechanical properties at the interface of fiber/matrix were observed to carbon-fiber composites because of preferential heating in the conductive fiber surface [69].

The change in properties of a polymer in the effect of ionizing radiation will strongly depend on whether the polymer chains goes to crosslinking or degrading. Radiation can cause both cross-linking and degradation, it depends on radiation dosage, polymer chemical structure, crystallite size, and temperature. The basic factor which will lead to degradation or crosslink is the chemical structure, for example, if the backbone of a polymer composed of saturated C-C linkage than predominantly it will undergo to crosslinking and if tertiary hydrogen replaced by an alkyl group as methyl cause degradation of the polymer matrix [64]. And if crystallite size is small that it is observed that it goes in an amorphous structure and ultimately increase the degradation probability under the influence of radiation. Depending on the effect of change, polymers are classified as degradable / scission polymers and cross-linking polymers. Polymers can be irradiated with alpha-rays, electron beam irradiation, gamma-rays, microwaves, X-rays, ultraviolet radiation etc. The large quantity of the biopolymers is degradable under the effect of radiation. Recent developments also proved that there are some biopolymers that can be crosslinked under high energy irradiation.

The polymer degradation causes the effect on macroscopic properties as a decrease in modulus and mechanical strength, electrical conductivity, color, and so on. These changes in the properties can be manipulated according to the area of application. It has already shown the effect of microwave-irradiated polymers on microstructural parameters as poly vinyl pyrrolidone/propyl methyl cellulose blends have been studied and observed that increased radiation dosage will not cause any increment in the photon energy of the microwave radiation [100]. Similarly, Polymer Microcapsules Containing Inorganic Nanoparticle studied using two polymer compounds, Poly sodium styrene sulfonate and poly allyl amino hydrochloride are irradiated with microwave radiations containing Ag as nano particles and without Ag. In the result, it was found that the complete destruction of polymer composites especially when it contained Ag because of high thermal and electric conductivity of Ag nano particles [101].

Microwave radiation interactions in polyvinyl chloride (PVC) graphite thick film resistors reported that a fall in resistance in high-value resistors and rise in resistance in low-value resistors with the microwave irradiation after a certain value depending upon the power and duration. It is also investigated that the decreases in resistance in HVR with time directed to a runaway process and increase in resistance in LVR leads to open circuits [102]. Similarly, the microwave absorption of pure paraffin can be improved by adding below 1%wt of nanoparticles. Carbon nanofibers and cobalt Nano enhanced the absorption capabilities as compared to pure paraffin. Furthermore, the heating rate shows a proportional relation with a concentration of nano particles which is a nice tool to control the system reaction. [103]Conversely it has shown that the significant increase in crystallinity upon high energy irradiation of high molecular weight polyethylene and further found the rise at ambient conditions aging [104]. Similarly, it has shown that upon gamma-irradiation the crystallinity and melting enthalpy increase because of crosslinking at high radiation dose.

Increase in crystallinity of biodegradable polymers such as polycaprolactone on exposure to U.V. radiation and further investigated that crystallinity increase with an increase in exposure time and after certain limit it starts decreasing [105].

CHAPTER 3

RESEARCH METHODOLOGY

3.1. Experimental Procedures

3.1.1 Materials

Poly (vinyl alcohol) 99% hydrolyzed (Mw= 89000-98000 g mole-1) was imported from Sigma-Aldrich Chemicals, USA. Graphene with 96-99% purity (size= 50-100 nm) was procured from Grafen Chemical Industries Co., Turkey. Materials were used for nanocomposite film preparation as received without any modification.

3.1.2 Preparation of Nanocomposite Films

PVA/graphene films were prepared using solution casting technique as shown in Figure 2. 3g of the polymer was dissolved in 50ml deionized water at 98^{o}C using magnetic stirrer (600 rpm). Then a certain amount of graphene (based on formulation ratio) was added into 25ml deionized water. A stable dispersion of graphene was achieved in water with ultra-sonication for 15 min at 30% amplitude using QSonica model Q700. After that, the dispersed filler was added to the PVA solution. Stirring of the mixture was continued for 1 hour at 80^{o}C. Then the mixture was degassed under vacuum for 10 minutes to remove the air bubbles from the solution. Finally, the mixture was poured into a plastic petri dish. Petri dish was placed on a levelled flat surface and allowed to dry at room temperature for six days. The dried nanocomposite films were carefully peeled off from the plastic petri-dish. Films were kept in a desiccator to avoid uptake. Different nanocomposites

films were prepared in the same manner with different graphene loadings. Table 1 provides the details of the prepared samples.

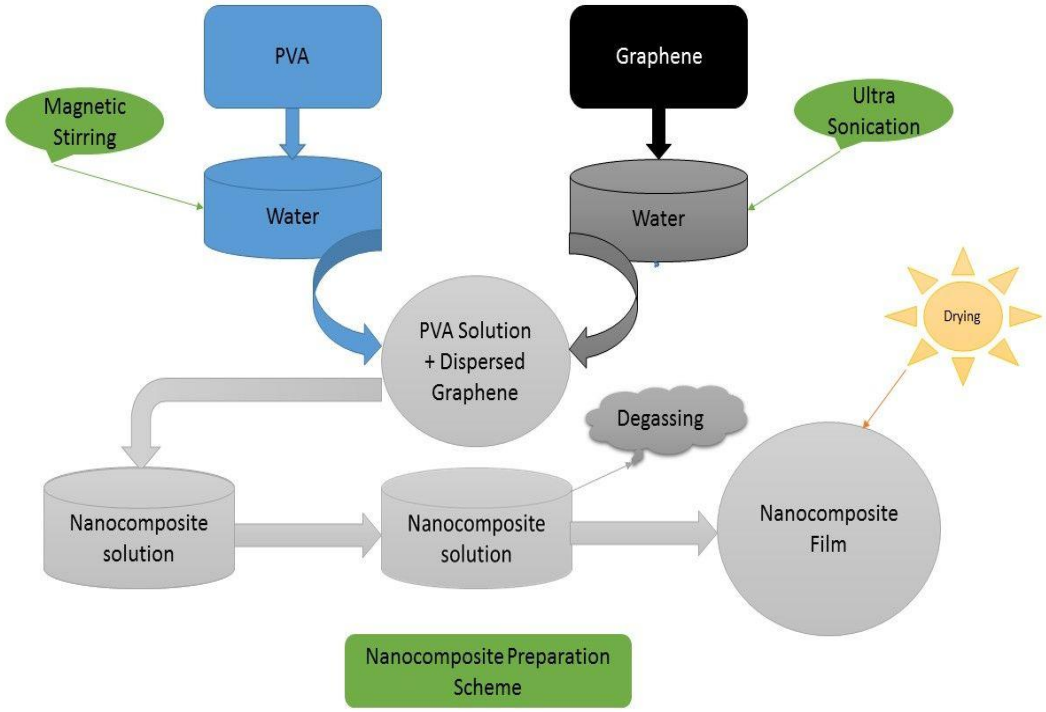

Figure 2: PVA / graphene nanocomposites preparation scheme.

3.1.3 Microwave Irradiation

Prepared samples were exposed to microwave radiations. Radiation was given using a domestic microwave oven in the presence of air at 200 watt power (2450 MHz frequency). Sample (size=30mm x 20mm x 6mm) was subjected to cyclic irradiation of 15 seconds by keeping graphene side towards the radiation source. After 15s sample was taken out from the oven to cool down at room temperature to eliminate the effect of heat. Irradiation durations were 5, 10 and 15 min. We could irradiate only neat polymer and 1% nanocomposite. 5% and 10% nanocomposites catch fire within 5s of radiation because of higher graphene concentration.

Table 1: Composition of PVA Nano-composites and irradiation time.

Sample Code	PVA (wt %)	Graphene (wt %)	Irradiation Time (min)	Water (mL)
P	100 (3)[a]	0 (0)[b]	0	75
P(5M)	100 (3)[a]	0 (0)[b]	5	75
P(10M)	100 (3)[a]	0 (0)[b]	10	75
P(15M)	100 (3)[a]	0 (0)[b]	15	75
G1	100 (3)[a]	1 (0.03)[b]	0	50+25
G1(5M)	100 (3)[a]	1 (0.03)[b]	5	50+25
G1(10M)	100 (3)[a]	1 (0.03)[b]	10	50+25
G1(15M)	100 (3)[a]	1 (0.03)[b]	15	50+25
G5	100 (3)[a]	5 (0.15)[b]	0	50+25
G10	100 (3)[a]	10 (0.3)[b]	0	50+25

[a ,b] Values in parentheses represent the weight in grams.

3.2. Characterization

3.2.1 Differential Scanning Calorimetry (DSC)

DSC-Q1000 of TA instrument was used for the study of isothermal crystallization kinetics and percentage crystallinity. DSC was carried out under 50 mL/min flow of nitrogen. The machine was calibrated through Indium melting characteristics. About 4-6mg sample weight was taken for each individual DSC run. Heat-cool-heat cycle was employed at constant heating and cooling rate of 10 ^{o}C/min. Each sample was heated from room temperature to 250^{o}C and kept isothermal for 3min at 250^{o}C to minimize the effect of thermal history. After that sample was cooled to 30^{o}C and again heated up to 250^{o}C. Data of second heating cycle was used for analysis. To ensure the reproducibility all experiments were conducted three times. Percentage crystallinity was calculated using below relationship (1) [106].

$$x = \int_{T}^{T\infty} \frac{\left(\frac{dH}{dT}\right) dT}{161} \times 100 \qquad (1)$$

Where the enthalpy of melting for 100% crystalline PVA is 161 Jg^{-1}.[107]

DSC was also used for isothermal crystallization kinetics. About 4-6mg sample was heated at a constant rate of 15^{o}C/min to 250^{o}C then kept isothermal for three minutes. After that sample was cooled at the high rate of 100 ^{o}C/min to a specified temperature Tc. Than sample kept isothermal for enough time (t_c) to achieve constant line of the exothermic signal. Relative crystallinity can be calculated using the following relationship (2).[108]

$$\alpha(t) = \frac{\Delta H(t)}{\Delta H(total)} = \int_{to}^{ti} \frac{\frac{dH}{dt}dt}{\int_{to}^{t\infty} \frac{dH}{dt}dt} \quad (2)$$

Where ΔH (t) is related to the exothermic value of heat at time t, while ΔH (total) is the heat released against the complete isothermal crystallization process. dH referred as the small quantity of heat released against infinitesimal interval of time dt. Universal Analysis 2000 software was used for the calculation of running integral and baseline. Following relationship (3) was used to get the volume fraction from the mass fraction.

$$X_t = \frac{\alpha(t)}{\alpha(t) + (\frac{\rho c}{\rho a})(1 - \alpha(t))} \quad (3)$$

Where ρ_c is the density for fully crystalline poly (vinyl alcohol), ρ_a is the density for fully amorphous poly (vinyl alcohol). Respective values of these densities are 1.345 $g.cm^{-3}$ and 1.269 $g.cm^{-3}$[109].

3.2.2 Thermogravimetric analysis (TGA)

Thermal degradation kinetics was studied using SDT Instrument thermogravimetric analyzer (Q600). Samples of 5-6 mg weight were heated at a constant heating rate of 10 ^oC / min from room temperature to 600 ^oC under the 100mL/min flow of nitrogen.

3.2.3 Fourier transform infrared (FTIR)

The study of both original and radiated samples functional groups was done by using Nicolet 6700 Fourier Transform Infrared (FTIR). The spectra were recorded in the band range of 400-4000cm^{-1}.

3.2.4 Raman Spectroscopy

Raman spectra of the samples were obtained by Horiba Jobin Yvon Raman spectrometer (iHR320) with CCD detector. The spectra were taken in the range of 100-3000 cm-1 with the resolution of 532nm. The exposure time was 30 s and the laser intensity was 60%.

3.2.5 Scanning electron microscope (SEM)

The scanning electron micrographs were taken from Tescan, MIRA 3 LMU FTIR. Samples were coated for surface analysis with 5 nm thick gold coating using sputter coating under vacuum.

3.2.6 X-ray Diffraction (XRD)

XRD spectra of the samples were taken with Bruker D8-Advance X-ray diffractometer using CuKα radiation with a wavelength of 1.5414A^{o}. To detect any crystal structure changings the angle of diffraction (2Ɵ) was varied from 5^{o} to 60^{o}.The XRD spectra were taken with a scanning rate of 2^{o}/min operating at 30kV and 30mA.

3.2.7 DC Conductivity

DC conductivity of the composite films was measured using Keithley 2400 source meter. The samples were prepared as a rectangle of 2cm long and 1cm wide. Two point method was adopted

for measurement. DC conductivity of each sample was calculated by measuring the electrical resistance using equation (4).

$$\alpha = \frac{L}{R.A} \tag{4}$$

Where α, R, L, and A represent the resistivity, resistance, length and cross sectional area of the sample respectively.

3.2.8 Electromagnetic Interference Shielding Effectiveness (EMI SE)

EMI SE of the un-irradiated and irradiated samples was measured at the X-Band 8-12GHz using two port Hewlett Packard (HP) 8510C vector network analyzer. Standard wave guide transmission line and rectangular holder were utilized to take the both forward and backward scattering (S) parameters. 85054D Agilent Technologies calibration kit was employed prior to EMI SE measurement in order to eliminate any disturbance created by the transmission line and rectangular holders. EMI SE is calculated from measured S-parameter based on equation (5) [110].

$$SE_T(dB) = 10log.\frac{1}{|S_{21}|^2} = 10log.\frac{1}{|S_{12}|^2} \tag{5}$$

3.2.9 Ultimate Tensile Strength (UTS)

Tensile properties were measured using Universal Testing Machine (UTM), Instron 3366. ASTM D638-10 standard was used with ramp velocity of 5mm min^{-1}. Dumbbell-shaped samples were prepared as per ASTM D638. The test was repeated three times for the calculation of appropriate parameters and the average values are listed in this article. The reproducibility of the results with ±5% accuracy was confirmed

CHAPTER 4

RESULTS AND DISCUSSIONS

4.1. FTIR Analysis

Figure 3 (A) represents the spectra of pure PVA and PVA/graphene un-irradiated samples. Figure 3 (B) represent the spectra of un-irradiated and irradiated PVA samples, while Figure 3 (C) represent the spectra of un-irradiated PVA and irradiated nanocomposites. Characteristic broad peak across 3200-3500 cm^{-1} correspond to stretching vibration of an alcoholic hydroxyl group (-OH) of PVA and nanocomposites [111]. The peak around 2814-2970 cm^{-1} represents the alkyl (C-H) stretching. Carboxylic group (C=O) stretching vibrational peak around 1743 cm^{-1} is due to graphene while the hump at 1712 cm^{-1} is because of C=O group in PVA. Hydroxyl group (-OH) in-plane blending and C-H wagging in pure PVA is in the band of 1487-1230 cm^{-1} while stretching vibration of nanocomposites –OH group is at 1384 cm^{-1}. Epoxy (C-O-C) stretching at 1240 cm^{-1} is due to graphene (fuller-enol) while vinyl group (C=C) stretching from 1140-955 cm^{-1} is due to pure polymer. Stretching vibration of C-O from 973-870 cm^{-1} and out of plane vibration of C-C at 840 cm^{-1} is because of pure PVA. It can be seen that the intensity of absorption spectra, from 3200-3500 cm^{-1} due to –OH group of pure PVA, decreases with increase in graphene percentage (Figure 3 (A)). This is because of the H-bonding interaction of oxygenated group in graphene and –OH of PVA at cost of already existing inter and intra H-bonding. This phenomenon usually referred as hydrogen bond barrier [21], [112]. Decrease in the intensity and shifting was also observed against C-H and C=O bands because of scissoring mode. These results confirmed the interaction between the polymer (PVA) and filler (graphene) [83], [113]. PVA mobility is effected due to these H-bonding interaction can be observed by the changes in the transition behavior (glass transition

temperature T_g). It can be seen clearly from Figure 3 (B), that after 5 min of irradiation, the intensities of vinyl (C=C) and carboxylic (C=O) group increases due side chains scission which may facilitate the formation of cross-linking structure. Similar changes have been observed for irradiated nanocomposites compare to the neat polymer as shown in Figure 3 (C). The higher irradiation (10 and 15) mins showed some overlapping between the bands of C-H (aliphatic), HC=O (aldehyde) and –OH (hydroxyl) 3500-2970 cm^{-1} [114]. Further in 10 min and 15 min irradiated samples carbonyl group peak intensity decreased, compare to 5 min irradiated sample, along with overlapping which is due to backbone rupture of polymer trunk. FTIR results are in agreement with previously reported results in which PVA undergo rupture and structure arrangement due to gamma-irradiation as per following scheme (6) [66], [114]–[116].

$$(C = COH)_n + (radiation) - H_2O \rightarrow (C = CHO)_{n-m} + (C = CHO)_m \qquad (6)$$

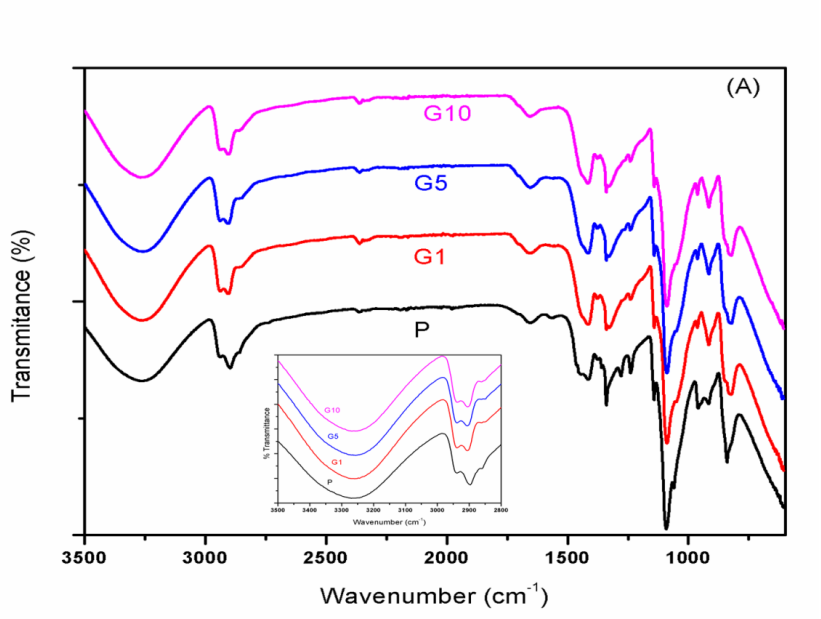

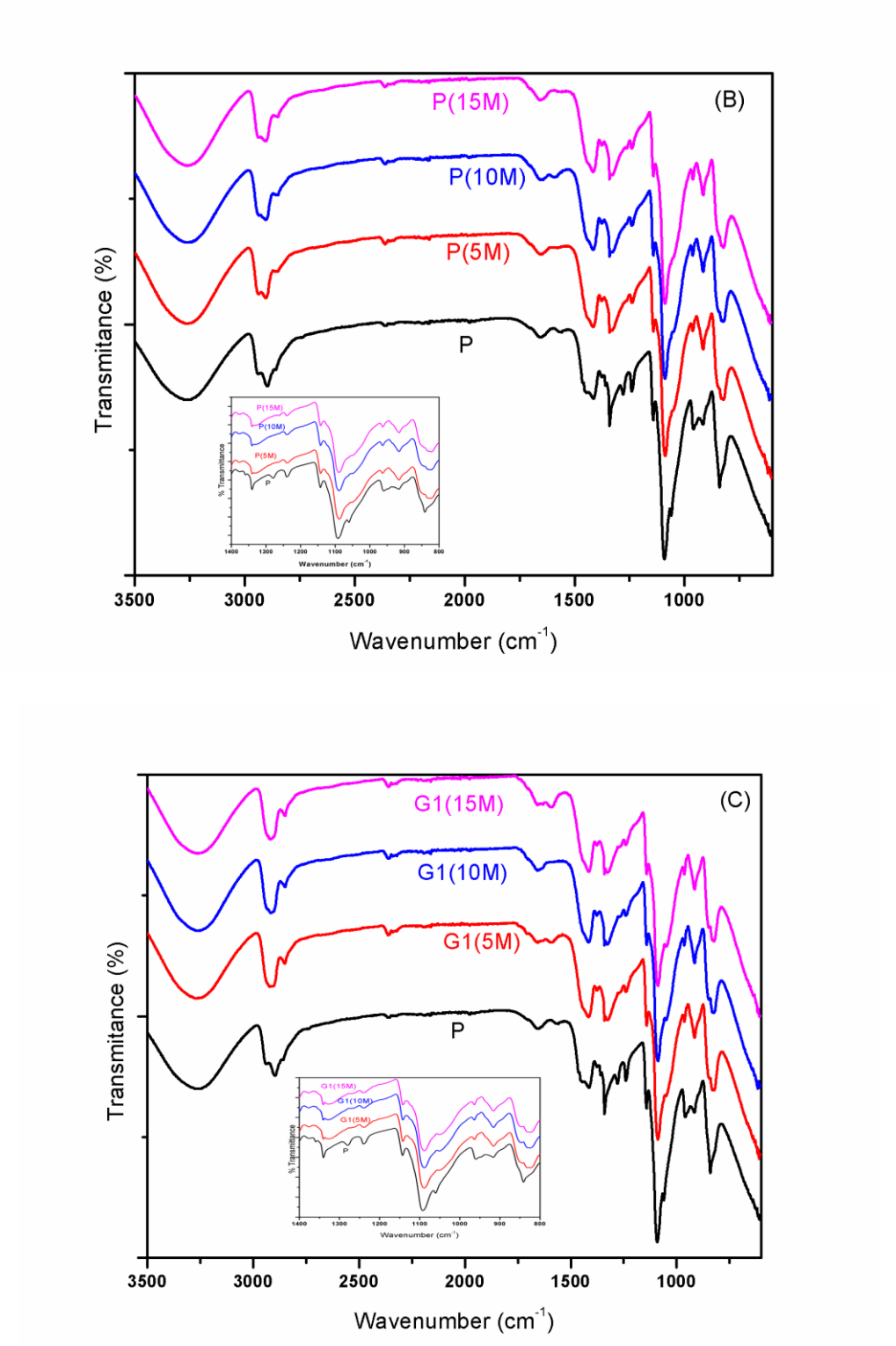

Figure 3: FTIR-spectra (A) PVA, PVA/graphene nanocomposites; (B) PVA and PVA irradiated samples; (C) PVA and PVA/graphene irradiated samples.

4.2. Raman Analysis

Figure 4 (a-b) displays the Raman spectra of un-irradiated and irradiated nanocomposites. D-band, G-band, and the 2D band are the three important characteristic peaks of Raman spectra. D-band corresponds to the out-plane breathing mode of sp2 atoms and indicates the level of defects present in graphene structure [117]. G-band is associated to the E2g phonon at the center of Brillouin zone [118]. As shown in Table 2 the intensity of D-band increases with the increase graphene content in PVA-graphene nanocomposites. This indicates the formation of defects in graphene structure which may facilitate the improvement in the interaction of graphene with the polymer chains via covalent bonding [119].

In the case of irradiated nanocomposites, after 5 min of microwave irradiation of nanocomposite (Figure 4 (b)), a significant increase in the intensity of D-band was observed. The D-band intensity increased from 69.17 to 126.70 after 5min of irradiation of G1. This is associated with the formation of defects in the graphene structure by irradiation. In addition the I_D/I_G was also increased from 0.31 to 0.55 after 5 min of irradiation (Table 2) The increase in I_D/I_G was demonstrated by Ferrari and Robertson hypothesis (that the crystalline structure of graphene transform to nano crystalline). The structural changes in graphene induced by irradiation lead to improvement in exfoliation of graphene and better interaction via chemical bonding with PVA chains as observed in FTIR analysis. Thus results in more stronger and thermal stable nanocomposite. However, further irradiation of G1 at 10 min and 15 mins leads to decrease in the I_D/I_G ratio as shown in Table 2. The decreasing behavior of I_D/I_G ratio suggests the transformation of nano crystalline structure of graphene to amorphous phase at higher irradiation time. This may results in the weak and poor interaction of graphene with PVA chains and leads to lowers the thermal stability of nanocomposite as further supported by thermal analysis.

Table 2: I_D/I_G ratio of un-irradiated and irradiated nanocomposite

Sample	D-Peak (-1357)	G-Peak (-1583)	I_D/I_G
G1	69.17	216.58	0.31
G5	74.42	227.23	0.32
G10	87.32	192.34	0.45
G1(5M)	126.70	229.94	0.55
G1(10M)	76.41	229.10	0.33
G1(15M)	67.72	255.76	0.26

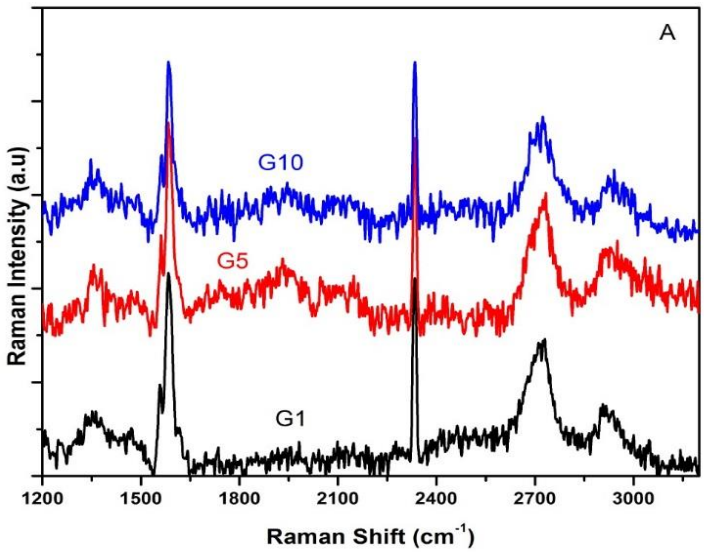

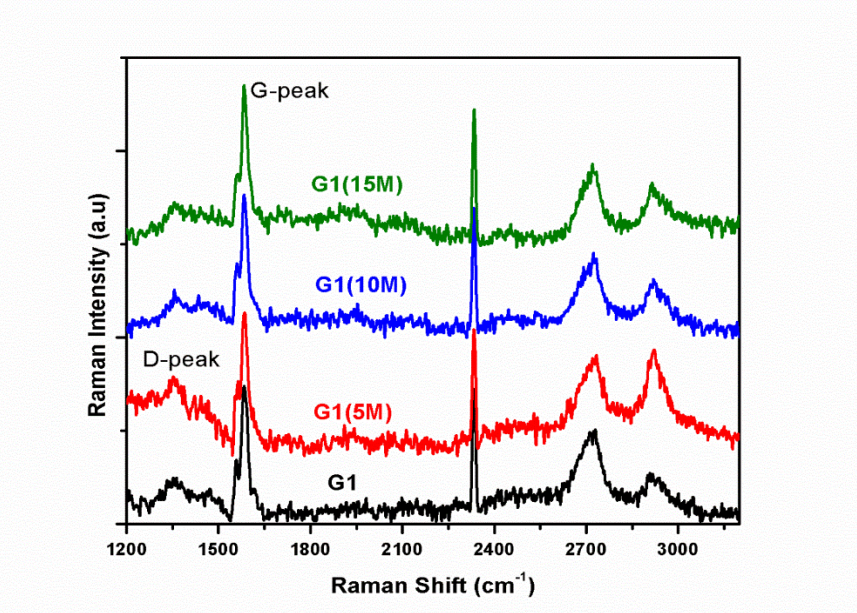

Figure 4: Raman spectra of un-irradiated nanocomposite (a) and irradiated nanocomposite (b).

4.3. SEM Analysis

SEM images of the surfaces of the PVA and PVA/graphene nanocomposites before and after irradiation are shown in Figure 5 & Figure 6 respectively. From Figure 5 (A-D) it can be seen that with the incorporation of graphene in PVA matrix, the smooth surface of PVA changed to rough and discrete patterns. This may be attributed to graphene enrichment in PVA chain which became more prominent with a higher concentration of graphene. In addition, the difference in structure can be observed by comparing *Figure 5* (D) (graphene enrich side) and Figure 5 (D') (polymer enrich side of the same G10 nanocomposite). SEM images of irradiated samples were taken at lower voltage with higher magnification to avoid deterioration and to show degradation respectively. Figure 6 (E-G) clears demonstrates that after 5min of irradiation, the smooth surface of PVA showed some erosion which may result in the development of cross-linking in P (5M) followed by the degradation in P (10M) and P (15M) at 10 and 15 min of irradiation respectively.

In addition, in the case of the nanocomposite, the rough and discrete patterns of un-irradiated G1 (Figure 5 (B)) changed to very smooth and continuous surface after 5 min of irradiation. This may be associated with the formation defects in graphene structure (as confirmed by Raman analysis) and chain scission of PVA chain which results in an increase in graphene polymer interaction and ultimately effect the crystallinity and thermal stability as discussed below. Moreover, higher irradiation (10 and 15) min gradually increased the rupture of G1 (10M) and G1 (15M) surface (Figure 6 (I-J)). This is the indication of degradation which leads to decrease in percentage crystallinity and thermal stability of the nanocomposite. Moreover, these morphological changes produce an interesting alteration in electrical and mechanical properties of the composites.

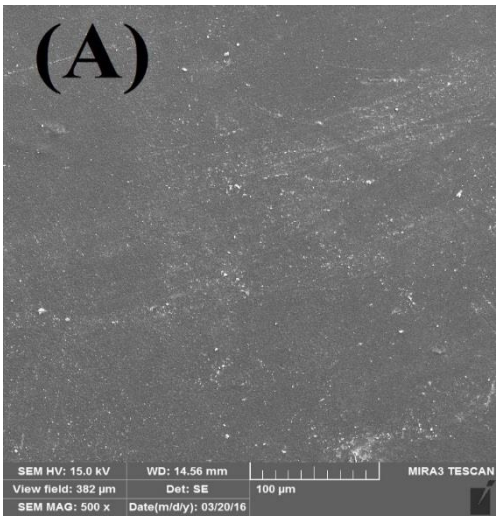

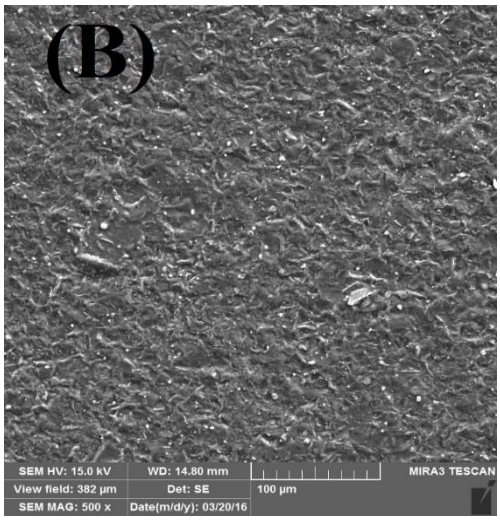

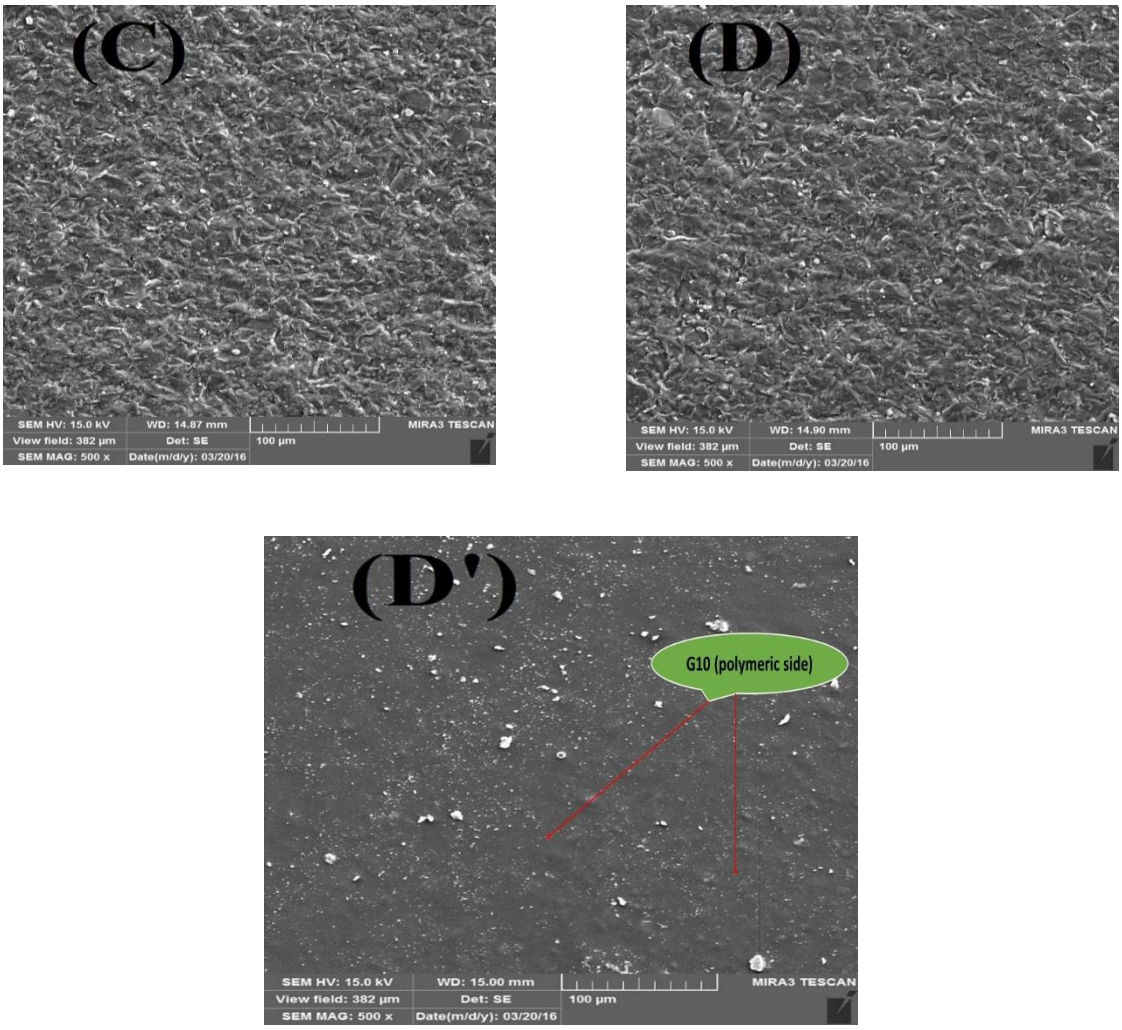

Figure 5: Surface view of un-irradiated samples, (A) P, (B) G1, (C) G5, (D) G10, (D') G10 (polymer enrich side).

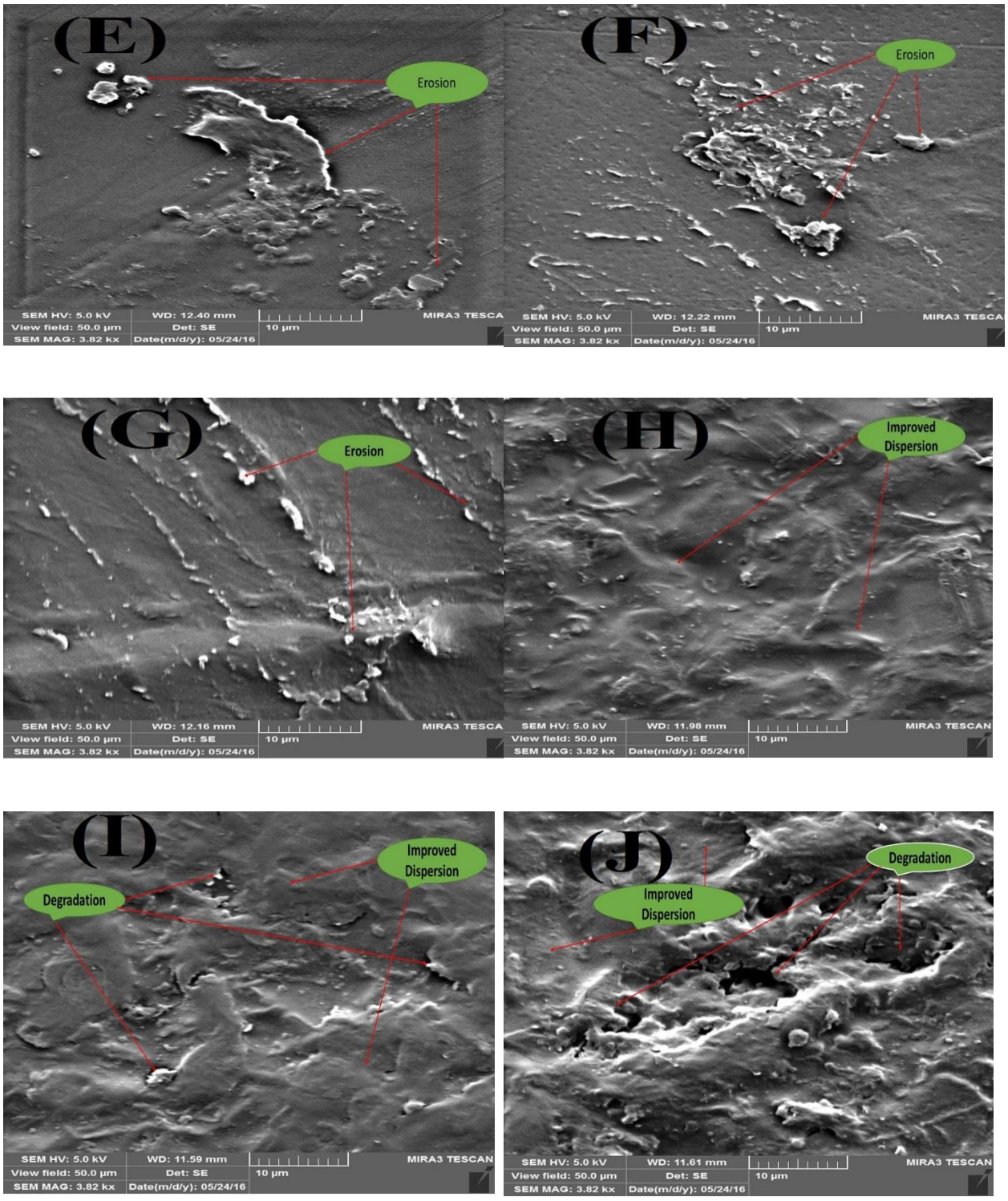

Figure 6: Surface view of samples irradiated (E) P (5M), (F) P (10M), (G) P (15M), (H) G1 (5M), (I) G1 (10M), (J) G1 (15M).

4.4. XRD

X-ray diffraction study is a useful tool to investigate the amorphous and crystalline nature of the polymer and composites. The XRD patterns of un-irradiated and irradiated samples shown in Figure 7. Pure graphene shows a crystalline peak at $2\Theta = 26.4^{o}$. PVA matrix shows a semi-crystalline peak at $2\Theta = 20^{o}$ while this peak shifted at $2\Theta = 19.5^{o}$ in G1, G5 and G10 along with graphene peak at $2\Theta = 26.4^{o}$ which intensity is increasing with graphene percentage.

Figure 7 (b) shows XRD patterns for un-irradiated and irradiated pure PVA. A crystalline peak can be seen at $2\Theta = 29^{o}$ in irradiated samples which intensity is decreasing when radiation time increase from 5min to 15min along with a semi-crystalline peak at $2\Theta = 20^{o}$ as present in un-irradiated PVA sample. The semi-crystalline peak also suppressed with an increase in radiation time which indicate the conversion of semi-crystalline structure to amorphous. The additional peak in irradiated samples also describes the change in structure caused by radiation. Hence, for pure PVA sample 5min irradiation change the structure to more crystalline compare to un-irradiated sample while the amorphous nature of the polymer matrix increase with an increase in radiation duration [120]. Similarly, Figure 7 (c) shows the XRD patterns for G1 un-irradiated and radiated samples. The peak at $2\Theta = 19.5^{o}$ in G1 shifted to $2\Theta = 20.4^{o}$ after irradiation along with an increase in intensity. Moreover, this increase in intensity suppressed when irradiation time increased from 5min to 15min. The intensity of the graphene peak present in G1 also decreased with increase in irradiation time which indicate the dispersion improvement (as conformed from SEM analysis) along with irradiation time. These XRD patterns variation indicate the modification in the microstructure of PVA/graphene composite which exhibits interesting changes in mechanical and electrical properties.

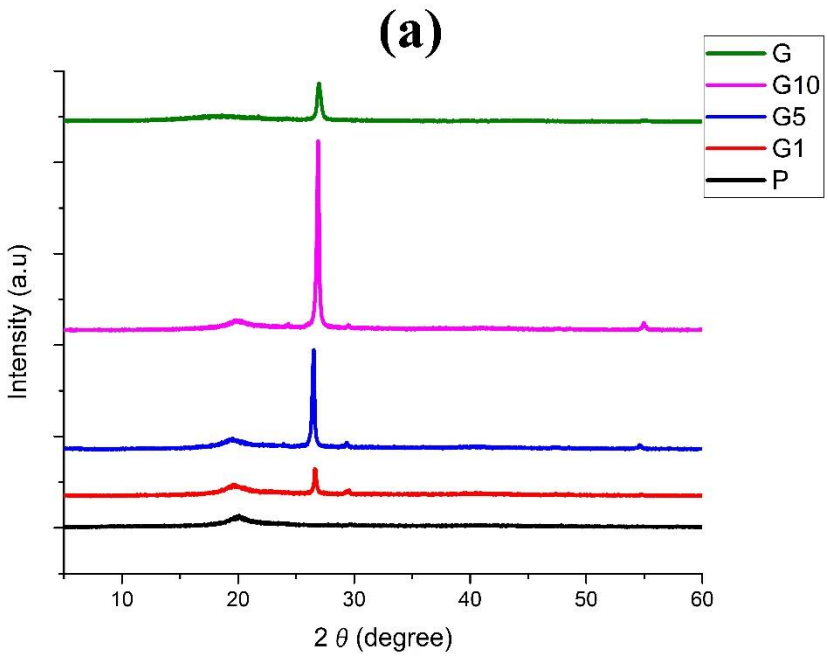
(a)
G
G10
G5
G1
P
Intensity (a.u)
10
20
30
40
50
60
2 θ (degree)

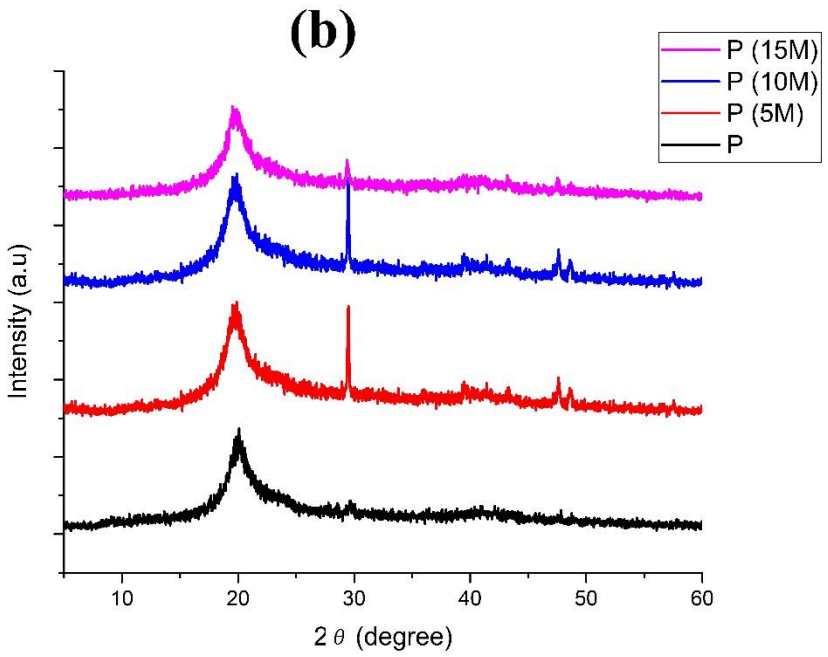
(b)
P (15M)
P (10M)
P (5M)
P
Intensity (a.u)
10
20
30
40
50
60
2 θ (degree)

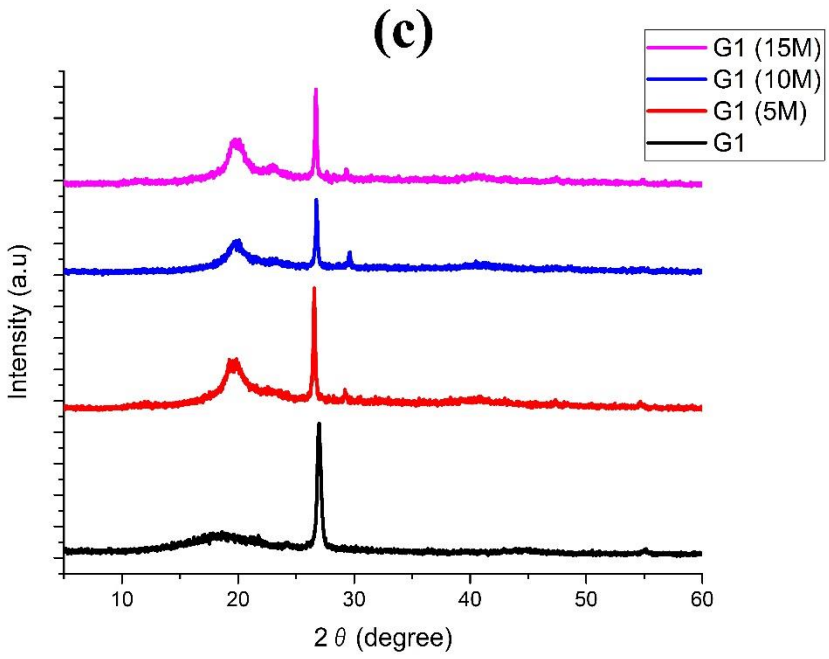

Figure 7: The XRD patterns of pure PVA, graphene, un-irradiated, and radiated samples.

4.5. Crystallinity

The effect of graphene on the percentage crystallinity of PVA was studied with the help of DSC. DSC data is summarized for original and irradiated samples in Table 3. The decrease in the degree of crystallinity has been observed with the incorporation of graphene. For example, the degree of crystallinity of PVA decreased from 55% to about 46% with the incorporation of 1% graphene. The reduction continues with an increase in graphene contents (Table 3). Due to the high aspect ratio of graphene, it penetrates and form hydroxyl bonding with OH group of PVA as indicated in FTIR results and restricts the dynamic movement of PVA chains in the nanocomposite. This restriction in dynamic movement causes the decrease in crystallinity. Similar results have been reported in literature for various polymer-graphene nanocomposites [87], [121], [122].

After irradiation, the percentage crystallinity of PVA remains almost constant (Table 3). In contrast, 5 mins irradiation of G1 nanocomposites showed a substantial increase in crystallinity [66]. The degree of crystallinity of G1 increased to about 9% after 5 mins of irradiation. Low irradiation exposure (5min) of G1 results in chain-scission produced short length PVA chains and defect in graphene [70]. Therefore chances of better chain arrangement of PVA chain and interaction of graphene with polymer matrix arises within the polymer nanocomposite [70], [123]. This increase in percentage crystallinity is also attributed to recrystallization of molecular chains under the influence of radiations [124]. However, higher irradiation (10 and 15) mins caused intense degradation of PVA chains and crystalline graphene structure which consequently reduces the crystallinity of G1 [125]. Moreover, the melting point of G1 was decreased with irradiation (Table 3). As both crosslinking and degradation destroy the crystallographic phase which eventually causes the decrease in melting point.

Table 3: Percentage crystallinity and melting point (T_m) of original and irradiated samples.

Sample	**% Crystallinity**	**T_m (°C)**	**Sample**	**% Crystallinity**	**T_m (°C)**
P	55	229	**G1 (5M)**	55	229
P (5M)	56	228	**G1 (10M)**	49	227
P (10M)	56	228	**G1 (15M)**	49	225
P (15M)	54	226	**G5**	43	231
G1	46	230	**G10**	41	232

4.6. Isothermal Crystallization Kinetics

Differential scanning calorimetric was used for isothermal crystallization kinetics of PVA, PVA/graphene original and irradiated samples. Avrami model was utilized for this purpose [27]. Avrami model relates the transformed volume fraction (X_{t-to}) with time ($t-t_o$) taking lamellar crystal growth and nucleation rate into account. Following Eq.4 is the mathematical form of Avrami model [26].

$$X_{t-to} = 1 - e^{-(K(t-to))^n} \quad (7)$$

Where X_{t-to} is the transformed volume fraction, n referred as Avrami exponent which is the function of nucleation process, K is rate constant of crystallization and t_o entitled as induction time. 'n' provide the qualitative details of growth and nucleation process. Linearize form of Eq.4 is as follow;

$$Ln\big(-Ln(1 - X_{t-to})\big) = nLn(t - t_o) + Ln(K) \quad (8)$$

Avrami exponent *n* and *K* were calculated by drawing plot between *Ln (-Ln (1-X_{t-to}))* and *Ln ($t-t_o$)*. Where the slope gives the value of n and intercepts provide the value of *K*. Isothermal crystallization kinetics were performed at different temperatures [26]. Eq. 2 and 3 were used to determine the transformed volume fraction. Results are listed below in Table 4 and Avrami linearized plots are shown in Figure 8. The data fitting was done in a range of 3-50 % of relative crystallinity. From Table 4 it can be seen that $t_{1/2}$ for pure PVA is higher than nanocomposites due to slow crystallization. The process of crystallization become faster in nanocomposites because of nucleation effect of graphene [126]. In the case of G5 and G10 $t_{1/2}$ is higher than G1 which indicates the slow overall crystallization rate. It is due to agglomeration of graphene particles at a

high percentage of filler in the nanocomposites. This agglomeration becomes more prominent in G10 which ultimately lower down the crystallization process, resulting in a higher $t_{1/2}$.

Table 4: Avrami analysis outputs for PVA and PVA/graphene original and irradiated samples.

Sample	**T_c**	**n**	**K x10^3**	**$t_{1/2}$**	**Sample**	**T_c**	**n**	**K x10^3**	**$t_{1/2}$**
	^oC		**min^{-n}**	**min**		**^oC**		**min^{-n}**	**min**
P	215	1.89	11.05	8.99	**G1(5M)**	215	2.32	6.15	7.63
	214	2.22	14.51	5.74		214	2.05	13.76	6.86
	213	2.18	27.77	4.39		213	2.25	192.98	1.77
	212	2.24	80.31	2.62		212	2.05	86.52	2.76
	211	2.24	151.25	1.97		211	2.26	320.16	1.41
P(5M)	215	2.11	5.69	9.82	**G1(10M)**	215	2.32	6.15	7.63
	214	2.25	13.08	5.88		214	2.22	10.98	6.46
	213	2.21	29.27	4.18		213	2.14	28.46	4.45
	212	2.20	82.13	2.64		212	2.61	65.58	2.45
	211	2.12	199.89	1.79		211	2.35	215.65	1.64
P(10M)	215	2.12	5.55	9.78	**G1(15M)**	215	2.05	9.08	8.23
	214	2.07	13.01	6.85		214	2.26	34.20	5.82

	213	2.25	31.48	3.96		213	2.15	26.67	4.54
	212	2.19	59.89	3.05		212	2.41	38.74	3.30
	211	2.30	154.19	1.92		211	2.29	126.06	2.11
P(15M)	215	2.00	8.29	9.92	**G5**	215	2.18	13.89	6.00
	214	2.11	25.45	4.82		214	2.26	27.61	4.17
	213	2.24	32.40	3.93		213	2.23	42.07	3.53
	212	2.28	84.90	2.52		212	2.25	74.57	2.70
	211	2.31	143.66	1.97		211	2.23	310.51	1.43
G1	215	1.84	43.63	4.49	**G10**	215	2.31	28.08	7.17
	214	2.19	57.22	3.14		214	2.33	116.68	5.95
	213	2.25	139.52	2.04		213	2.09	117.86	4.05
	212	2.25	751.70	0.96		212	2.32	467.08	2.85
	211	2.04	1040.51	0.82		211	2.42	591.14	1.07

The values of $t_{1/2}$ of irradiated samples are higher as compared to un-irradiated. This increased in $t_{1/2}$ value is due to crosslinking within the irradiated sample. Crosslinking reduces the chain mobility resulting in a slower crystallization process [127], [128]. The Avrami exponent n for all the samples is varying between 1.9 to 2.4, which indicate the two dimensional growth of

morphology as reported earlier for PVA [129]. Figure 9 represent the experimental and model predicted relative crystallinity versus time. It can be seen that isothermal crystallization kinetics can be perfectly described by the Avrami model for the PVA and PVA/graphene nanocomposites.

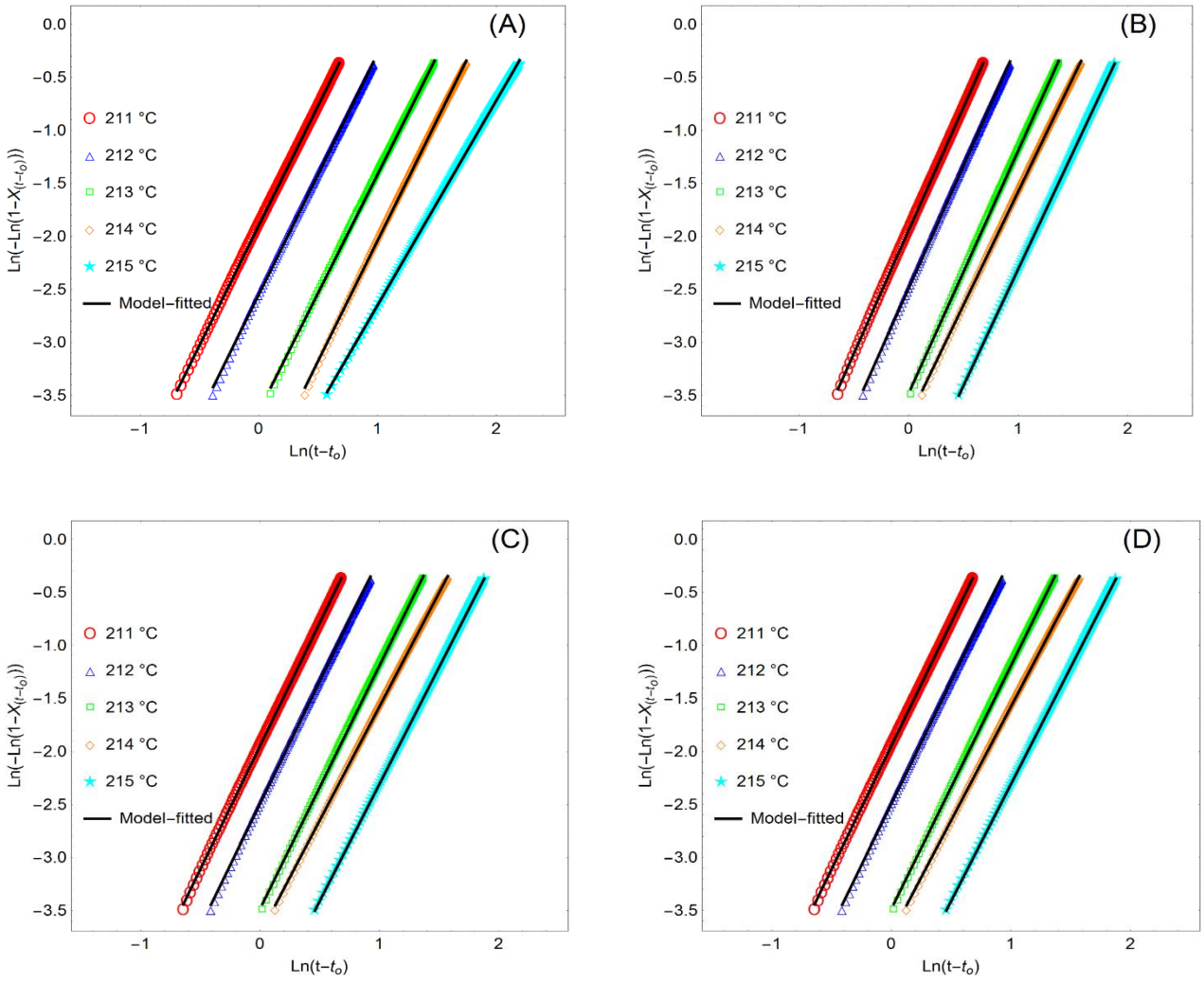

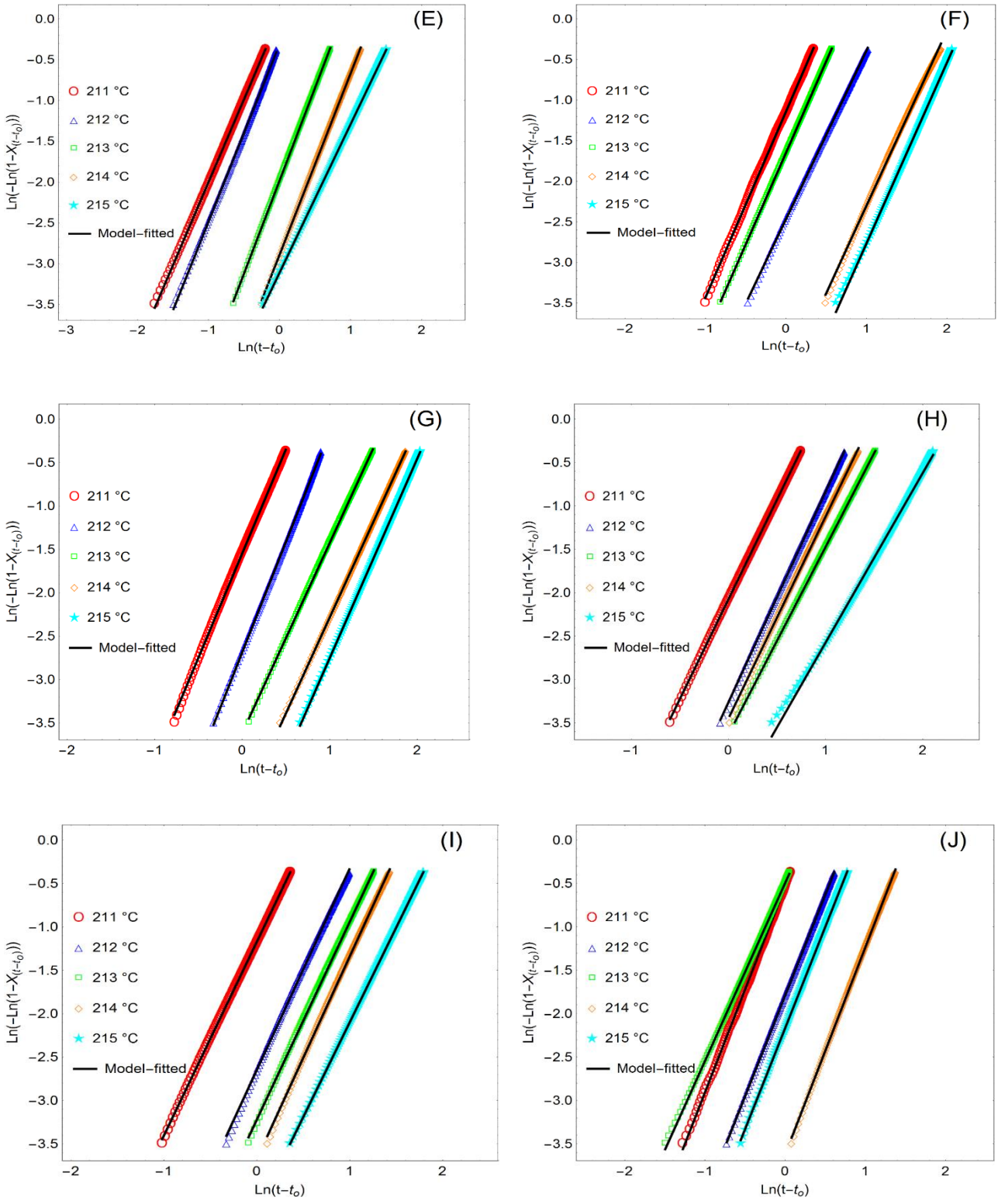

Figure 8: Avrami model linearized plots for (A) P, (B) P (5M), (C) P (10M), (D) P (15M), (E) G1, (F) G1 (5M), (G) G1 (10M), (H) G1 (15M), (I) G5, (J) G10.

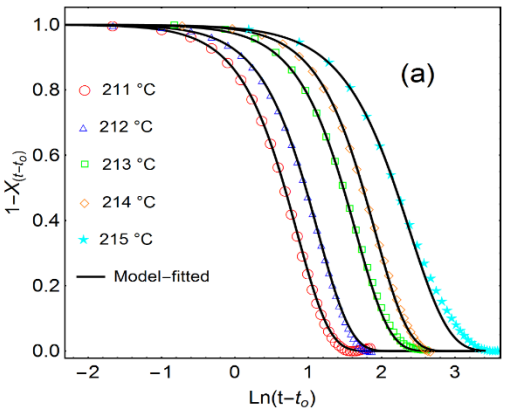
(a)
211 °C
212 °C
213 °C
214 °C
215 °C
Model–fitted
1–X(t–to)
Ln(t–to)

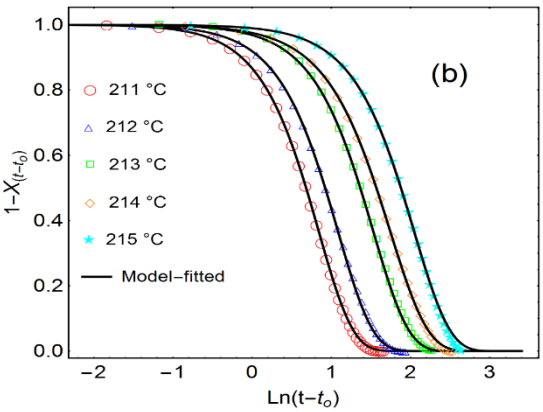
(b)
211 °C
212 °C
213 °C
214 °C
215 °C
Model–fitted
1–X(t–to)
Ln(t–to)

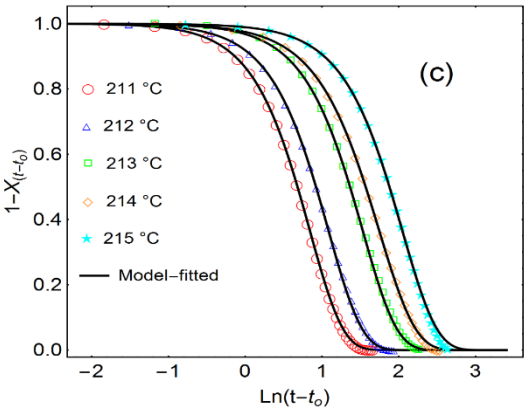
(c)
211 °C
212 °C
213 °C
214 °C
215 °C
Model–fitted
1–X(t–to)
Ln(t–to)

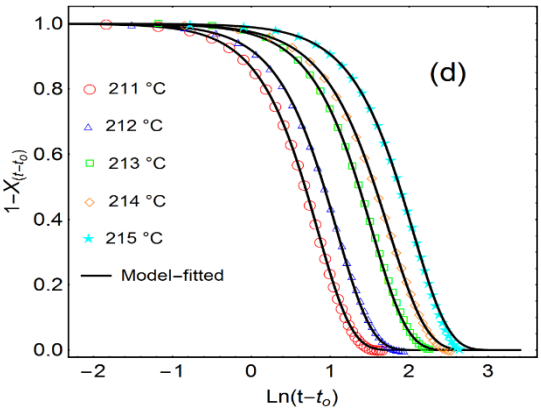
(d)
211 °C
212 °C
213 °C
214 °C
215 °C
Model–fitted
1–X(t–to)
Ln(t–to)

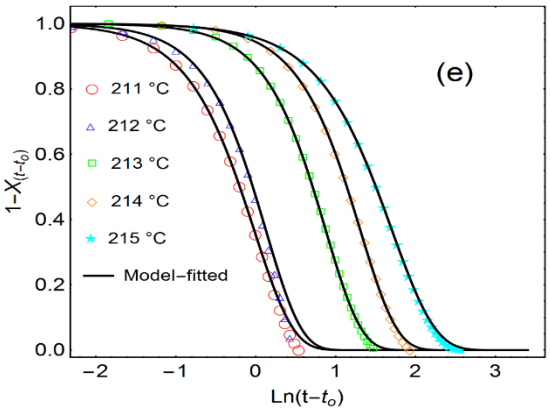
(e)
211 °C
212 °C
213 °C
214 °C
215 °C
Model–fitted
1–X(t–to)
Ln(t–to)

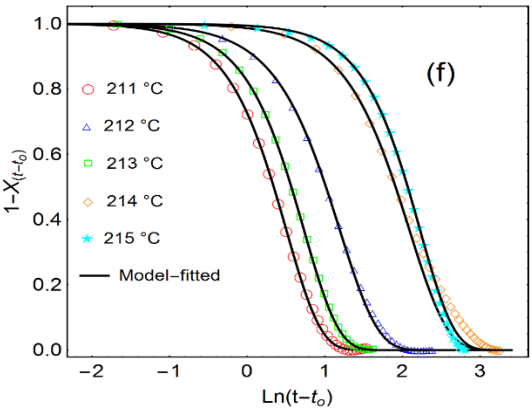
(f)
211 °C
212 °C
213 °C
214 °C
215 °C
Model–fitted
1–X(t–to)
Ln(t–to)

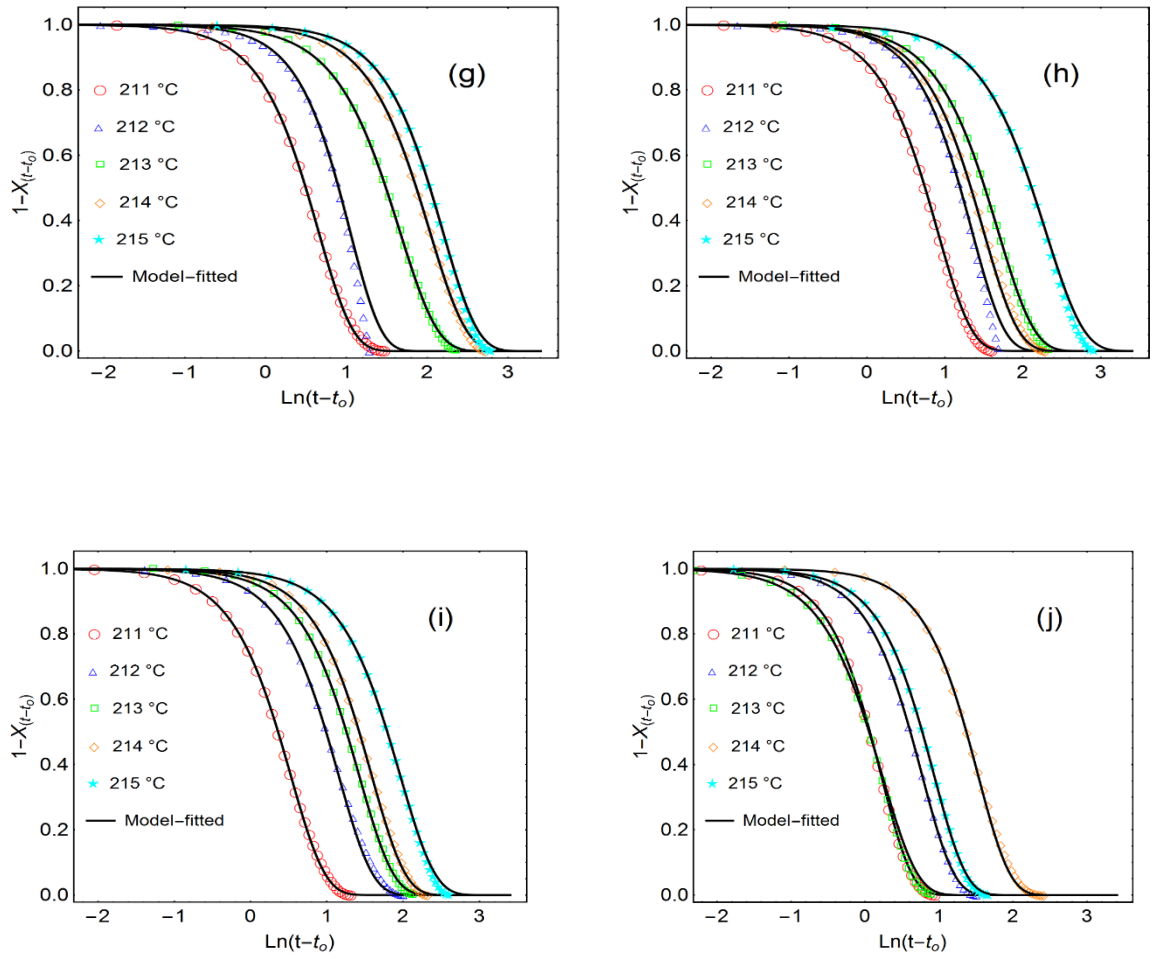

Figure 9: Graduate development of crystallinity against time from Avrami model-fitted and experimental values (a) P, (b) P(5M), (c) P(10M), (d) P(15M), (e) G1, (f) G1(5M), (g) G1(10M), (h) G1(15M), (i) G5, (j) G10.

4.7. Nucleation Efficiency (η_{nu})

Graphene nucleation efficiency was also studied. The following relationship 6 was used to calculate the nucleation efficiency:

$$\eta_{nu} = \frac{T_{c,N} - T_{c,PVA}}{T_{c,SN} - T_{c,PVA}} \times 100 \quad (9)$$

Where $T_{c,\,N,}$ and $T_{c,\,PVA}$ are the respective peak crystallization temperatures of PVA/graphene (original and irradiated) composites and pure PVA. $T_{c,\,SN}$ represent the self-nucleated PVA melt peak crystallization temperature [130]. For the calculation of $T_{c,\,SN}$ pure PVA (controlled sample) was heated up to 228 ^{o}C in partial melt state at the constant heating rate of 10^{o}C/min [131], [132]. The sample was kept isothermal for five minutes and then cooled at the rate of 10^{o}C/min up to 0^{o}C. Recorded $T_{c,\,SN}$ was 202.8 ^{o}C. Favorable interaction within the crystal fragments and molten polymer in the presence of fragmented crystallites are referred as an ideal process for self-nucleation. The values for $T_{c,\,peak}$ and η_{nu} are listed in the below Table 5. From Table 5 more than 100% efficiency for all PVA/graphene nanocomposites can be observed. This effectiveness is attributed to the high aspect ratio of graphene as compare to pure PVA crystals. These unique characteristics of graphene cause the decrease in free energy barrier and ultimately effect on the process of crystallization at higher temperature [133]. The decreases in nucleation efficiency in 5% and 10% nanocomposites is due to agglomeration of graphene nano-particles at high percentages. In the same way, the increase in nucleation efficiency of 5 min irradiated sample is attributed to improvement in the dispersion of graphene within the composite. However, 10min and 15min irradiated samples are showing a decrease in efficiency due to degradation. These results are in accordance with FTIR and SEM.

Table 5: Graphene nucleation efficiency in the PVA/graphene nanocomposites

Sample	**$T_{c,peak}$ (^{o}C)**	**η_{nu}**
P	202	0

G1	204	420
G1(5M)	204	547
G1(10M)	203	152
G1(15M)	203	149
G5	203	316
G10	203	103

4.8. Thermogravimetric Analysis (TGA)

The TGA scans of pure polymer and nanocomposites before and after irradiation were carried out for nearly 5-6 mg of samples. SDT Instruments thermogravimetric analyzer (Q600) was used under an inert atmosphere with 100 mL/min flowrate of nitrogen. Samples were heated at a constant heating rate of 10 ^{o}C / min from room temperature to 600 ^{o}C. Thermal decomposition of PVA and its nanocomposites comprises of four stages as show in Figure 10. The first stage before 230 ^{o}C is related to evaporation of trapped moisture within the samples. The second stage at ~235-300 ^{o}C corresponds to chain stripping mechanism due to the elimination of bound water. The third and fourth stages at ~340-520 ^{o}C are corresponded to samples pyrolysis which represents the chain-scission reaction (main degradation) by transfer of H_2 at scission site [134]–[136].

A decrease in thermal stability with the incorporation of graphene is clear from the obtained data. This decline in thermal stability is due to increase in thermal conductivity, nanocomposite heterogeneity and synergistic instability[137] between PVA and graphene. Graphene increases the

thermal conductivity of PVA which results in better heat conduction and therefore the degradation starts at earlier temperature. Decline in thermal stability can also due to graphene purity (~96%). As graphene used in the preparation of composites contains oxygen contents (~1-2% reported by the vendor). These oxygen contents produce different functional groups on graphene surface like ketone, hydroxyl, lactone epoxide, carboxylic acid, etc. which lower the thermal stability of pristine filler and ultimately of nanocomposites [121], [138], [139]. Similar results regarding the decrease in thermal stability with the incorporation of graphene / graphene-oxide with PVA and other hydrophilic polymers have been reported [121], [137], [140].

The other factor includes the structure of the nanocomposites. Produced films have two side one is graphene enrich while other polymer enriches as shown in SEM Figure 5 (D-D'). This structure facilitates agglomeration between the graphene contents. Agglomeration decreases the dispersion and resultantly gives intercalated rather than exfoliated structure. This produce uncoupled –OH group which produce initiating sites for rapid thermal decomposition. Many studies also have been made regarding the decrease in efficiency of filler due to lack of exfoliation in the structure [141], [142]. The increase in the thermal stability of G1 after 5min irradiation due to increase in dispersion and cross-linking. G1 (10M) show the decrease in activation energy as compare to G1 (5M) but due to still the presence of some crosslinked structure and just start of degradation its activation energy value is higher than G1. 15min irradiation cause the severe degradation, so, finally produce less thermally stable composite as G1 (15M).

Table 6: Thermal stat acquired from TG and DTG curves of neat and nanocomposite samples.

Sample Name	T_{on} (ºC)	$T_{50\%}$ (ºC)	T_{max} (ºC)
P	116	334	316
P (5M)	100	326	279
P (10M)	100	325	276
P (15M)	98	323	276
G1	106	303	279
G1 (5M)	110	306	281
G1 (10M)	107	305	281
G (15M)	106	302	280
G5	105	299	276
G10	104	294	268

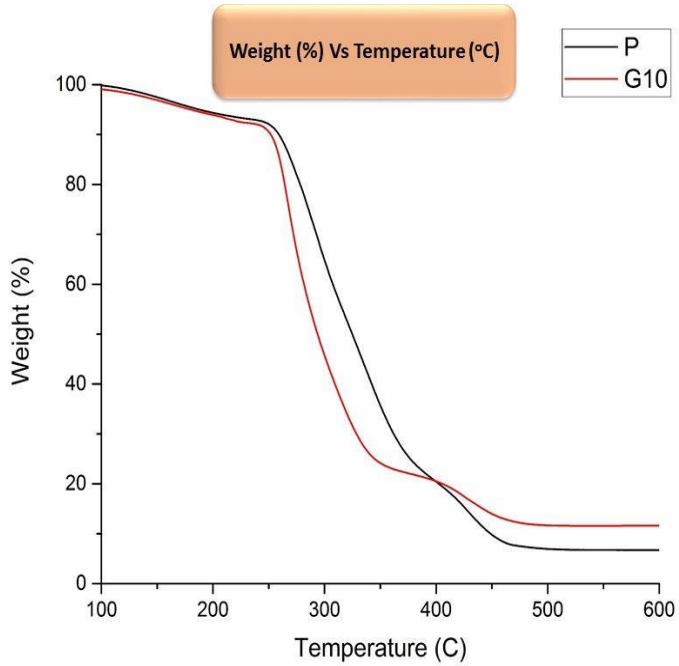

Figure 10: TGA curves for pure polymer (PVA) and 10% graphene nanocomposite: weight loss Vs temperature.

4.9. Thermal Degradation Kinetics

The thermal kinetics study provides the information about energy barrier and degradation mechanism of the process. There are a number of techniques have been used to study and analyze the non-isothermal degradation [143], [144]. A list of methods, differential and integral, have been proposed to calculate the kinetic parameters as reaction order (n), the rate constant (k) and activation energy (E) using thermogravimetric analyzer data with multiple or single heating rates. In the present study TGA data for neat PVA and PVA / graphene nanocomposite were fitted using nth order reactions models. The general equation is given as eq.10;

$$\frac{d\alpha}{dt} = kf(\alpha) \tag{10}$$

Arrhenius equation was used to calculate the temperature dependence of rate constant.

$$\frac{d\alpha}{dt} = k_o\, e^{\left(-\frac{E}{RT}\right)}.f(\alpha) \tag{11}$$

Where k_o is a pre-exponential factor, E is activation energy, R is the gas constant and α is fractional conversion. For nth order reaction model we have;

$$f(\alpha) = (1-\alpha)^n \tag{12}$$

For the non-isothermal process, we have below eq.

$$\frac{d\alpha}{dt} = \beta(\frac{d\alpha}{dT}) \tag{13}$$

Fractional conversion (α) is calculated by the following formula;

$$\alpha = \frac{m_o - m_i}{m_o - m_\infty} \tag{14}$$

Since the degradation is comprised of four stages, therefore first the degradation curve was divided into four separate steps with the help of peak fitting. Each stage then analyzed separately.

Since eq. 9 depends on two parameters "fractional conversion" and temperature. So, the experimental data was arranged in the form of (T, α, dα/dT) and fitting was done using Mathematica. The built-in command "***NonlinearModelFit***" was utilized and the final parameter as *n, k* and *E* were calculated. Although, the fitting process was done for the all four stages but we will keep our discussion to third and fourth steps (Chain-scission) which are the main degradation

stages [134]. Calculated parameters for all fourth stage are listed in below Table 7. Figure 11 show the conformity of experimental data with nth order reaction kinetics.

Table 7: Kinetic parameters for all four degradation stages.

Sample Name	**Stage**	**n**	**k**	**E (KJ/mole)**	**Sample Name**	**Stage**	**n**	**k**	**E (KJ/mole)**
P	1	1.33	5.9×10^{4}	46	**G1 (5M)**	1	1.31	2.6×10^{4}	43
	2	1.54	2.4×10^{15}	161		2	1.76	2.9×10^{24}	254
	3	1.47	2.2×10^{11}	130		3	1.45	4.7×10^{10}	128
	4	1.68	2.9×10^{17}	236		4	1.66	1.1×10^{15}	206
P (5M)	1	1.43	1.5×10^{4}	38	**G1 (10M)**	1	1.30	1.3×10^{4}	41
	2	1.57	3.0×10^{17}	182		2	1.67	7.8×10^{24}	259
	3	1.47	2.6×10^{11}	130		3	1.45	3.8×10^{10}	126
	4	1.61	3.0×10^{16}	224		4	1.76	8.6×10^{14}	204
P (10M)	1	1.33	7.1×10^{4}	45	**G 1(15M)**	1	1.33	5.5×10^{4}	45
	2	1.57	9.3×10^{17}	187		2	1.64	5.7×10^{22}	236
	3	1.45	2.2×10^{10}	129		3	1.45	3.4×10^{10}	119
	4	1.52	3.2×10^{15}	212		4	1.43	8.9×10^{12}	179

P (15M)	1	1.32	4.9×10^{4}	45	**G5**	1	1.31	2.4×10^{4}	44
	2	1.56	1.1×10^{17}	179		2	1.72	1.1×10^{28}	289
	3	1.46	1.0×10^{11}	128		3	1.47	4.3×10^{11}	124
	4	1.52	6.3×10^{14}	201		4	2.09	2.0×10^{14}	194
G1	1	1.29	8.9×10^{3}	39	**G10**	1	1.33	8.2×10^{4}	47
	2	1.65	6.1×10^{23}	247		2	1.64	3.9×10^{22}	229
	3	1.47	2.2×10^{11}	122		3	1.48	1.9×10^{12}	124
	4	1.65	2.1×10^{14}	197		4	1.92	1.4×10^{23}	178

It is clear from the data enlisted in Table 7 that incorporation of graphene in PVA slightly lowers the thermal stability. For example, the activation energy decreases from 131 KJ/mole to 124 KJ/mole in the third stage with the incorporation of 10% graphene contents. Similarly in fourth step activation energy decrease from 236 KJ/mole to 178 KJ/mole with the same 10% graphene contents. This is due to synergistic instability which decreases the thermal stability and ultimately lowering the activation energy. After irradiation, G1 show the increase in activation energy from 121.5 KJ/mole to 126.4 KJ/mole and 197.2 KJ/mole to 203.9 KJ/mole of third and fourth steps respectively. This increase in activation energy up to 10 min irradiation can be attributed to the structural changes resulting in the improvement of graphene dispersion within the nanocomposite. However, longer microwave irradiation (15 min) results in a decrease in the activation energy due to the degradation of the nanocomposite.

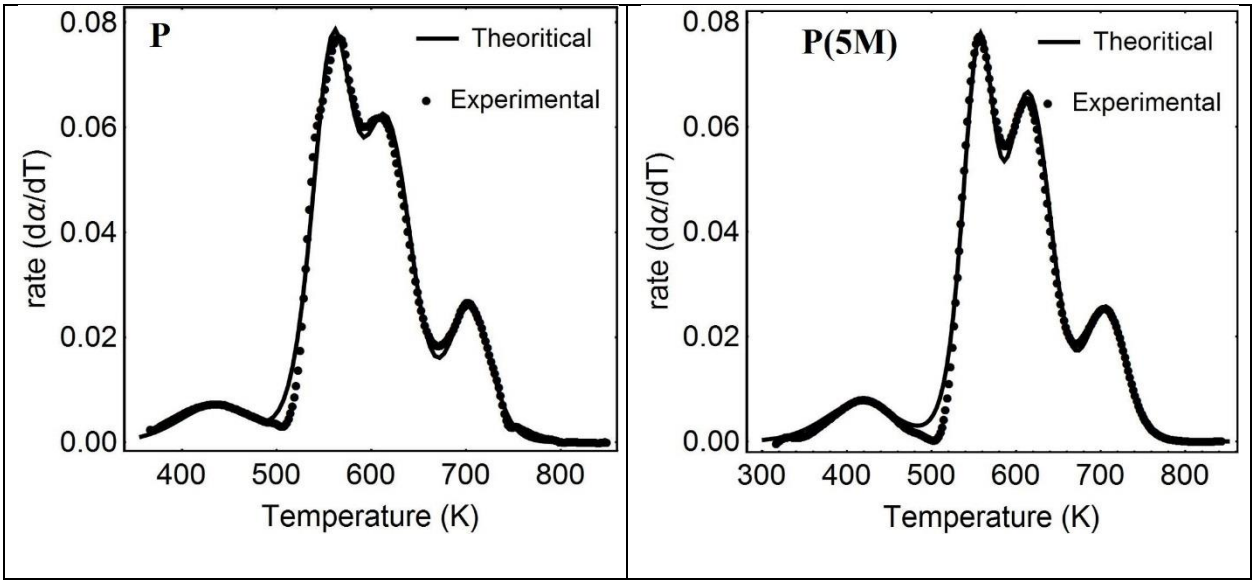

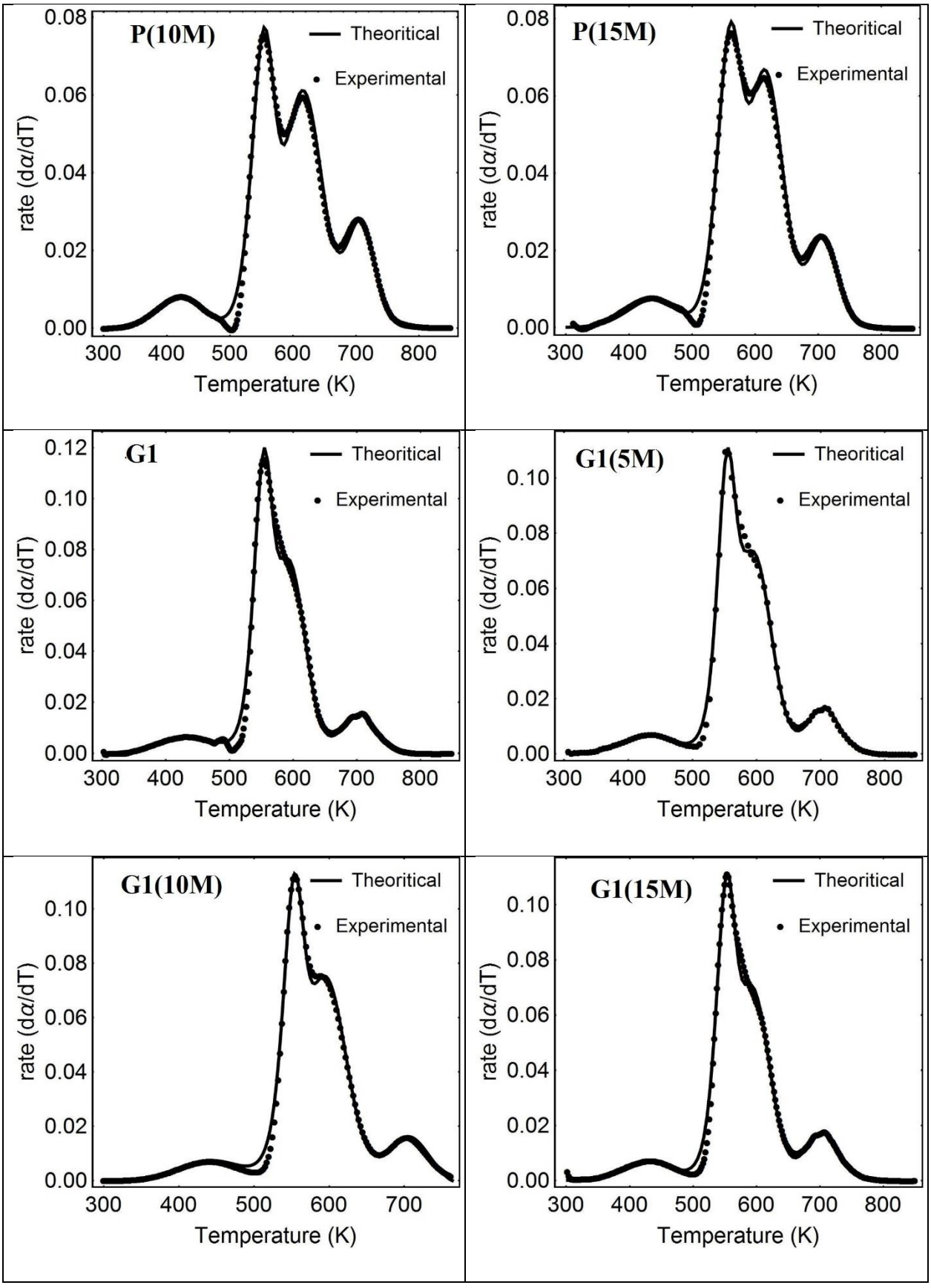
P(10M)
Theoritical
Experimental
rate (dα/dT)
Temperature (K)
P(15M)
Theoritical
Experimental
rate (dα/dT)
Temperature (K)
G1
Theoritical
Experimental
rate (dα/dT)
Temperature (K)
G1(5M)
Theoritical
Experimental
rate (dα/dT)
Temperature (K)
G1(10M)
Theoritical
Experimental
rate (dα/dT)
Temperature (K)
G1(15M)
Theoritical
Experimental
rate (dα/dT)
Temperature (K)

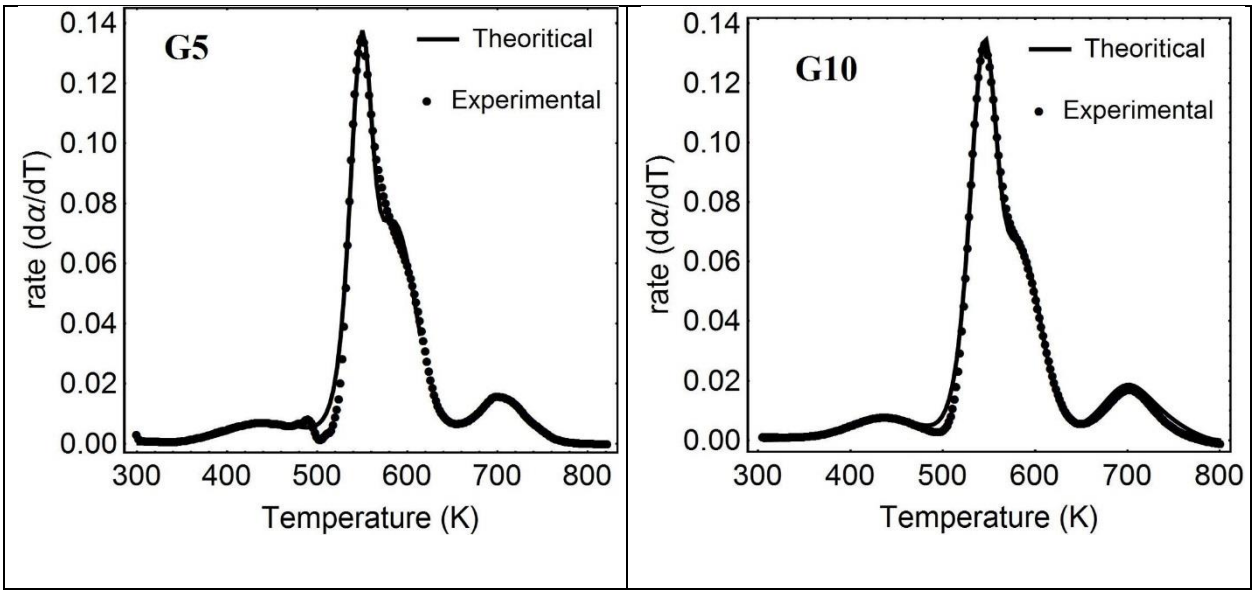

Figure 11: Conformity of experimental non-isothermal degradation kinetics with theoratical nth oreder reaction kinetics.

4.10. DC Conductivity

DC conductivity values of PVA/graphene un-irradiated and irradiated composites are listed in Table 8. Figure 12 depict the DC conductivity of the PVA/graphene composites with respect to graphene content. The DC conductivity of the composites increases with progressive increase in graphene content. The remarkable increase in DC conductivity value can be seen in the case of G5 compare to G1 followed by the high value of 3.55 S/cm for G10. Thus, percolation limit of the conductive system was reached at around 0.52-0.69 volume fraction of graphene. In the case of G1 PVA act as a continuous phase while in G5 and G10 graphene become the continuous phase. As π electron mobility is high in graphene thus increasing conductivity.

In the case of irradiated samples of G1, there is a slight increase in conductivity with irradiation time. This increase in conductivity is due to breakage of graphene clusters in G1 and subsequently improvement in dispersion due to irradiation as observed in SEM and XRD analysis.

Table 8: DC conductivity values for un-irradiated and irradiated samples.

Sample Name	DC Conductivity (S/cm)	Sample Name	DC Conductivity (S/cm)
P	0	**G1 (15M)**	0.039
G1	0.021	**G5**	2.17
G1 (5M)	0.027	**G10**	3.55
G1 (10M)	0.032		

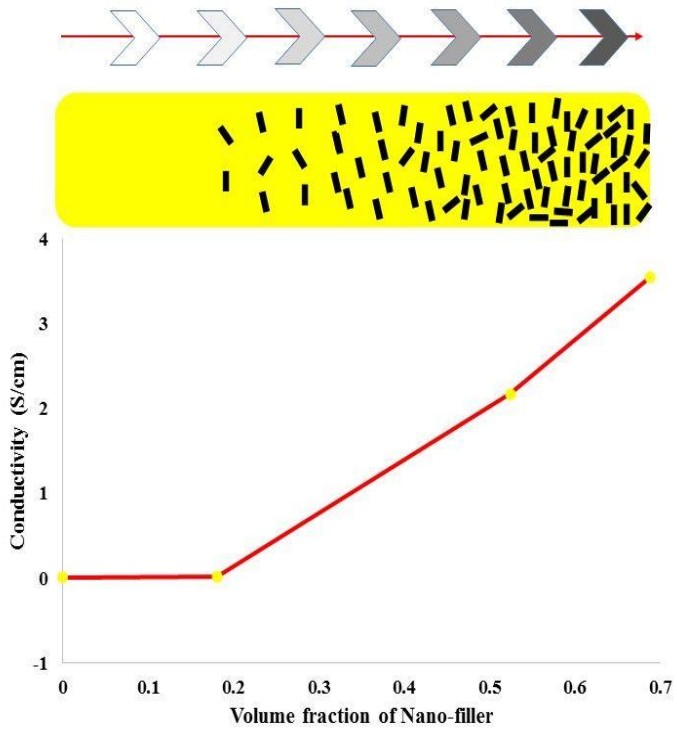

Figure 12: Dc conductivity of the PVA/graphene nanocomposites with respect to the volume fraction of graphene.

4.11. Theoretical Models for Prediction of DC Conductivity

DC electrical conductivity of the binary system, where nano-filler is a conducting phase while polymer matrix is an insulating phase, can be estimated from the application of different theoretical models. In this article, two such models as Bueche and Scarisbrick model have been implemented to predict the electrical conductivity of PVA/graphene nanocomposite. The pristine graphene conductivity value 100 S/cm [145] is used for modelling purpose.

4.11.1 Bueche Model

This model was proposed by Bueche for the prediction of the DC conductivity for two phase composite systems in which polymer act as an insulating phase while the conducting particles made the second phase. Mathematical expression for Bueche model is given in equation (15)[146];

$$\alpha_c = \alpha_f \upsilon_f + \alpha_p (1 - \upsilon_f) \quad (15)$$

Where α_c is the conductivity of the nano-composite system, υ_f is the volume fraction of the filler, α_f is the conductivity of the pristine nano-particles and α_p is the conductivity of the polymer. Conductivity values of the PVA/graphene composites were predicted using above equation (15).

Figure 13 shows the experimental and theoretical DC conductivity plots against volume fraction of graphene. The Large difference in both theoretical and experimental can be seen at low graphene content (before percolation) which reduces with the increase of graphene percentage within the composite system. Therefore, Bueche model does not predict correctly for the subjected system. Bueche model depend on the additive rule of mixing and this rule is appropriate for such systems in which the property difference in both phases should be low. In this case study, there is a large difference in electrical properties of PVA and graphene, especially conductivity. Therefore predicted DC conductivity values of the subjected system are mostly determine from the

conductivity of graphene. This is the main reason for the large difference in experimental and theoretical conductivity values.

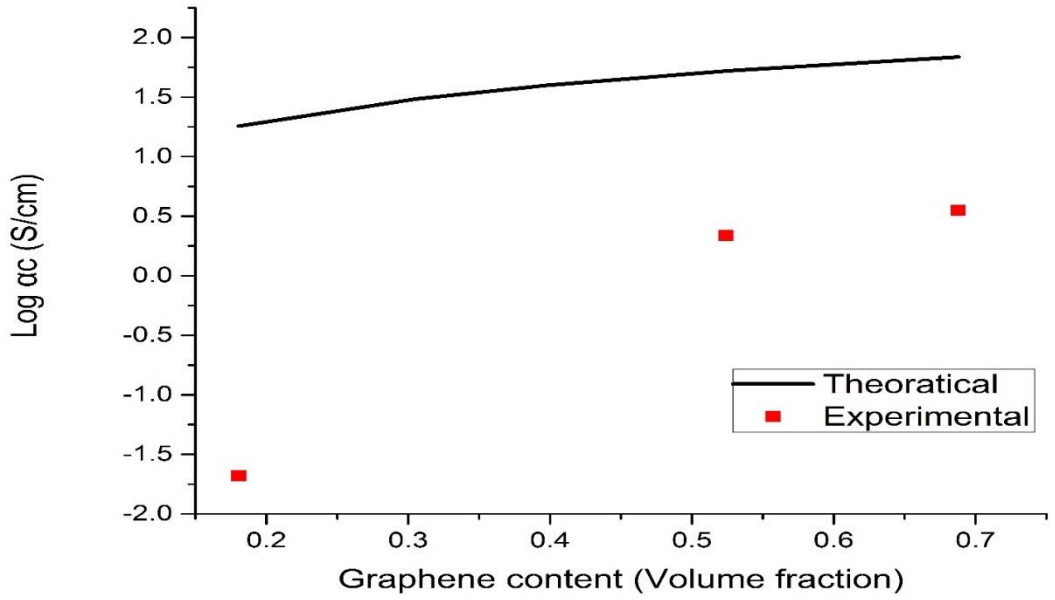

Figure 13: Experimental and theoratical DC conductivity (S/cm) against volume fraction of graphene for PVA/graphene composite system based on Bueche model.

4.11.2 Scarisbrick Model

This model is applicable for two phase composite system in which conducting particles scattered unsystematically in an insulating matrix. This model depends on conducting network generation probability by the contact of polymer and filler particles. Scarisbrick found that the electrical conductivity of the composites is the complex function of conducting filler concentration. Mathematically description of the model is given by equation (16) [59];

$$\frac{\alpha_c}{\alpha_f} = C^2 * v_f (v_f)^{v_f^{-2/3}} \qquad (16)$$

Where α_c is the conductivity of composite predicted by the model, α_f is the conductivity value of pristine filler, υ_f is the volume fraction of the nano-particles and geometrical factor C depends on the concentration of filler. Geometrical factor (C) depends on the overlapping and arrangement of the conducting chains in the matrix. Its value vary from 1 to 3×10^{-3}, thus the equation (16) can be re-write as follow;

$$\frac{\alpha_c}{\alpha_f} = \upsilon_f(\upsilon_f)^{\upsilon_f^{-2/3}}, \qquad Where\ C = 1 \tag{17}$$

$$\frac{\alpha_c}{\alpha_f} = 3\times10^{-3} * \upsilon_f\left(\upsilon_f\right)^{\upsilon_f^{-\frac{2}{3}}}, \qquad Where\ C = 3\times10^{-3} \tag{18}$$

Figure 14 shows the conductivity plots of experimental data and theoretical data calculated from Scarisbrick model at different values of C. It can be seen that there is a very close match between theoretical conductivity calculated by Scarisbrick model at C=0.1 and experimental conductivity mainly at a higher percentage of filler. Thus, this model is appropriate for a higher percentage of the conductive filler. Electrical conduction at high filler concentration is mainly due to the generation of the conductive network by the inter particle contact. The disadvantage of Scarisbrick model is that it has not accounted the conductivity of the polymer matrix (insulating medium) in the model. Thus, this model fails in the whole range of filler concentration as well as conductivity.

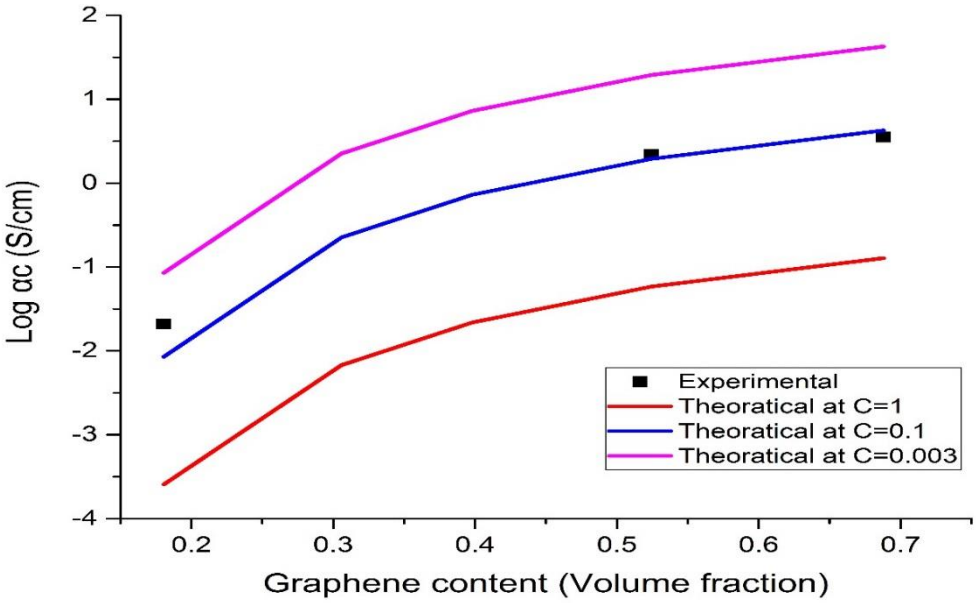

Figure 14: Experimental and theoratical DC conductivity (S/cm) against volume fraction of graphene for PVA/graphene composite system based on Scarisbrick model.

4.12. Electromagnetic Interference Shielding Effectiveness (EMI SE)

The EMI SE measured using vector network analyzer (VNA) for different nano-composites containing graphene over frequency in X-band. Estimation of SE over X-band frequency is that this range has practical significance and various military and commercial instruments operated under this range. The total SE can be estimated by scattering (S) parameters provided by VNA. Relationship (19) was utilized to calculate the SE.

$$SE_T(dB) = 10log.\frac{1}{|S_{21}|^2} = 10log.\frac{1}{|S_{12}|^2} \quad (19)$$

Where S_{12} and S_{21} correspond the coefficients of reverse transmission and coefficients of forward transmission, respectively. Figure 15 (a) describe the multiple attenuation mechanisms during SE measurement using polymer nano-composites containing conducting nano-filler. Figure 15 (b)

illustrate the measurement of S-parameters by a two port VNA. Figure 16 shows the EMI SE of un-irradiated samples while Figure 17 show the EMI SE of irradiated G1 samples. It is interesting to see that the SE of the composites increases with increase in graphene contents. The SE increase related to the increasing electrical conductivity [110]. Graphene nano-particles formed a continuous conducting network by distributing itself within the polymer matrix which behaves like a conducting mesh. Generally, the SE determines the mesh size as this mesh intercepts with electromagnetic radiations. By increasing the nano-filler contents produce more compact and fine mesh (as shown in SEM analysis) with the result of better SE [147]. However, higher loading imposes the adverse effect on mechanical properties of the nano-composites.

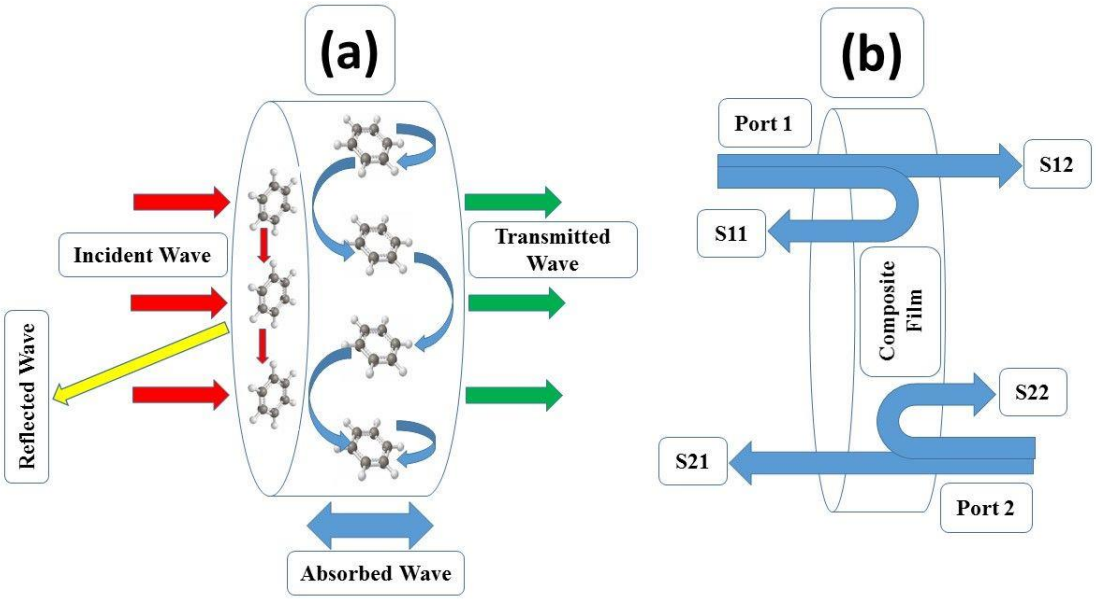

Figure 15: Schematic representation (a) Various mechanism of attenuation, (b) S-parameters in two ports vector network analyzer.

In the case of irradiated composites, it can be seen from Figure 17 that with the increase in irradiation time the EMI SE is increasing. This increase in SE correlated with improvement in

dispersion due to irradiation which results in better distribution of conductive filler in the polymer matrix. These results are analogous to SEM analysis and electrical conductivity. Thus interestingly, when prepared composites exposed to ionization radiations their capability to retard the effect of radiations or EMI SE increases with the passage of time along with conductivity.

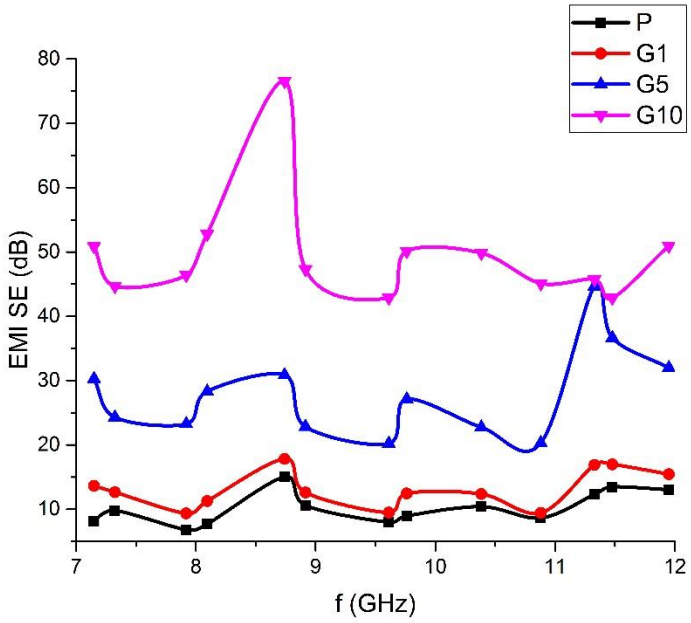

Figure 16: Electromagnetic interference shielding effectiveness (dB) of pure PVA and different PVA/graphene nano-composites versus frequency (GHz).

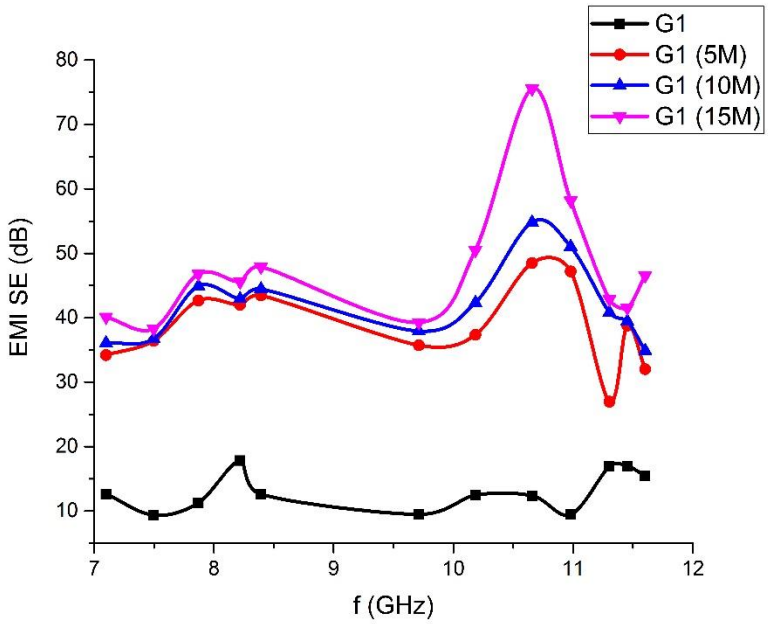

Figure 17: Electromagnetic interference shielding effectiveness (dB) of irradiated G1 samples versus frequency (GHz).

4.13. Mechanical Properties

The average values of ultimate tensile strength, modulus (Segment 0.00025mm/mm - 0.005 mm/mm) and yield strength of all samples are listed below in Table 9. Figure 18 shows (a) Tensile strength Vs graphene contents (P, G1, G5, G10), (b) Tensile strength Vs irradiation time (P, P(5M), P(10M), P(15M)), (c) Tensile strength Vs irradiation time (G1, G1(5M), G1(10M), G1(15M)). From Figure 18 (a) it can be seen that with the increase in graphene percentage in polymer matrix tensile strength and yield strength is decreasing.

This fall in tensile properties is due to agglomeration of nano-graphene particles within the polymer [21], [148]. From the XRD analysis, it is clear that by the increase in graphene percentage the characteristic peak of graphene appeared in G1, G5, and G10 which is the indicative of

agglomeration. This agglomeration propagates the weakening of interfacial adhesion between the polymer matrix and nano-sheets which caused the decrease in tensile properties. Moreover, the thickness of graphene enrich side is increasing with the increase of graphene percentage which facilitate the decrease in the tensile strength. In the case of irradiated P samples, there is a very small change in tensile strength. Tensile strength first increase after 5 min radiation then decrease gradually till 15 min irradiation. This change in tensile strength is related to structural changings as can be seen in XRD analysis. After 5 min irradiation, there is an increase in crystallinity of the sample from the mother matrix. This increase in crystallinity cause the increase in tensile strength [149], [150]. In the case of P (10M) and P (15M), the intensity of the peak decreases (structure transformation from more crystalline to amorphous) with irradiation time which results in the gradual decrease in tensile strength. Similarly, G1 irradiated samples show a slight change in tensile strength. This change in tensile strength attributed to structural transformation due to irradiation same as in P irradiated samples. XRD analysis for irradiated G1 samples conforms the increase in the intensity of PVA characteristic peak after 5 min irradiation which decreases after further irradiation. The decrease in tensile strength from G (5M) sample to G (15M) presumably because the degradation of polymer matrix and transformation of nano-crystalline structure of graphene to amorphous as confirm from Raman Spectroscopy[151].

Table 9: Tensile properties of irradiated and un-irradiated samples.

Sample Name	Tensile Strength (MPa)
P	46.0
P(5M)	46.6
P(10M)	45.8
P(15M)	45.8
G1	44.8
G1(5M)	45.1
G1(10M)	42.1
G1(15M)	41.6
G5	41.1
G10	40.9

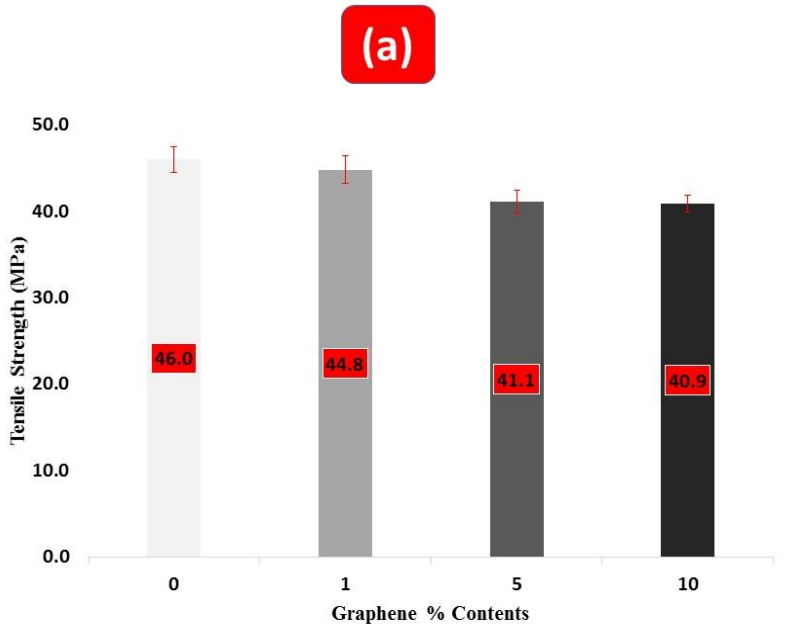
(a)
50.0
40.0
30.0
20.0
10.0
0.0
Tensile Strength (MPa)
46.0
44.8
41.1
40.9
0
1
5
10
Graphene % Contents

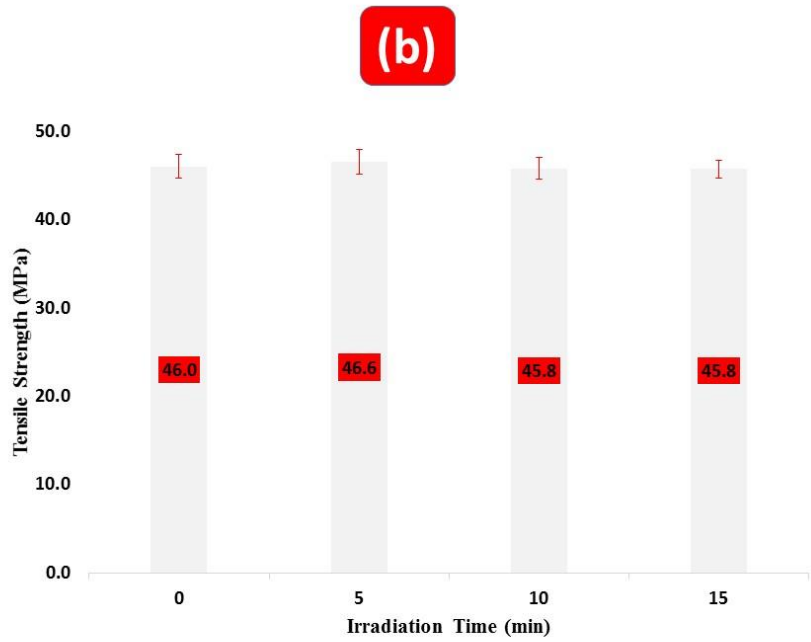
(b)
50.0
40.0
30.0
20.0
10.0
0.0
Tensile Strength (MPa)
46.0
46.6
45.8
45.8
0
5
10
15
Irradiation Time (min)

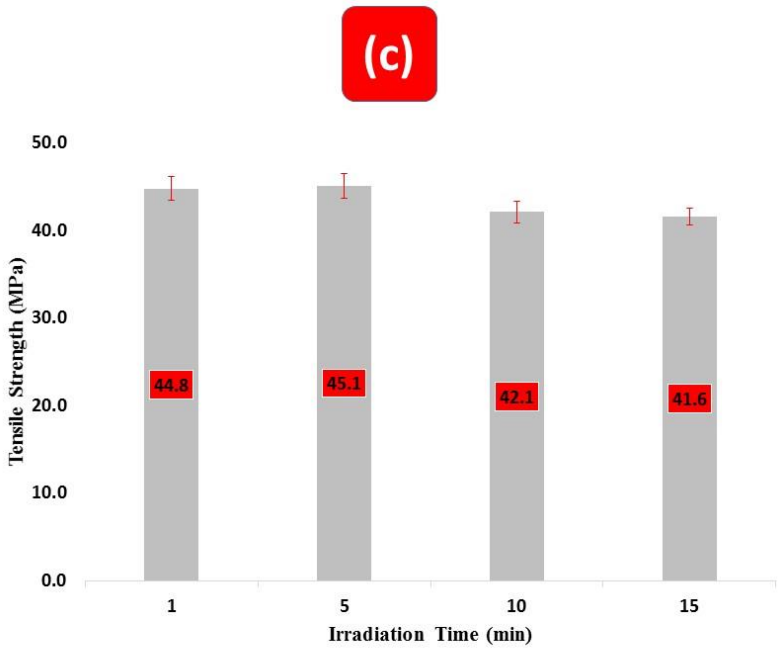

Figure 18: (a) Tensile strength Vs graphene contents (P, G1, G5, G10), (b) Tensile strength Vs irradiation time (P, P(5M), P(10M), P(15M)), (c) Tensile strength Vs irradiation time (G1, G1(5M), G1(10M), G1(15M)).

CHAPTER 5

CONCLUSION AND RECOMMENDATIONS

5.1. Conclusion

This study manifested the graphene and microwave radiations effect on electrical and mechanical properties of PVA composites. Reduction in crystallinity and thermal stability of PVA was observed with incorporation of graphene. The decrease in PVA crystallinity was due to restriction in the dynamic movement of chains. While synergistic instability between PVA and graphene slightly decreased the thermal stability. Microwave irradiation caused to increase the percentage crystallinity of G1 (5M) due to improvement in graphene dispersion. Similarly, a slight increase in percentage crystallinity after irradiation of neat polymer was also observed. 10 min and 15 min irradiation resulted in a decrease in the crystallinity of nanocomposite due to degradation of polymer chains and graphene crystalline structure. Moreover, improvement in thermal stability was found for G1 (5M) due to improved dispersion of graphene within the composite. Isothermal crystallization kinetics shows that the experimental data satisfied the Avrami model. Graphene incorporation increased the crystallization rate indicated by a decrease in $t_{1/2}$ and increase in crystallization rate constant. Thermal degradation kinetics for all the PVA and PVA/graphene nanocomposites were studied by the nth-order reaction kinetics. Kinetic parameters reaction order (n), the rate constant (k) and activation energy (E) were evaluated from thermal degradation kinetics. Calculated activation energy (E) from experimental data satisfied the findings regarding thermal stability of original and irradiated samples.

DC electrical conductivity of the PVA nano-composites was increased through the graphene incorporation. The composite system reached on the percolation threshold with 5% graphene contents in the matrix. This improvement in electrical conductivity is due to high π electron mobility in graphene which provides electricity transmission source in the composite system. It was analyzed that microwave irradiation improved the DC conductivity of the G1 (15M) composite from 0.021 S/cm to 0.039 S/cm after 15 min due to dispersion improvement of nano-filler. Better agreement was found between the experimental conductivity and theoretically predicted conductivity by Scarisbrick at C=0.1. The Bueche model fails to correctly predict the conductivity because of the additivity in mixing rule. This mixing rule is applicable for that binary system which has more a less similar conductivity values. Similarly, electromagnetic interference shielding effectiveness improved strikingly by the incorporation of graphene nano-particles which formed a continuous conducting network by distributing itself within the polymer matrix and behave like a conducting mesh. EMI SE enhancement was also observed in irradiated samples due to breakage of filler clusters which result in better distribution and more intercept with electromagnetic radiations. The decrease in tensile properties was found with the increase in graphene incorporation in the composite system. This fall in tensile properties is due to agglomeration of nano-graphene particles within the polymer matrix along with increase in thickness of graphene enrich side. Moreover, the tensile strength of the irradiated samples increased further after 5 min irradiation due to the transformation of structure to more crystalline. However, further irradiation up to 15 min lead to decrease in the tensile strength due to degradation of polymer matrix.

5.2. Recommendations

From our research work we recommend to study the effect other irradiation techniques such as a laser, UV, gamma rays, etc. to see their effect on composite films. Moreover the biodegradability test of the prepared samples.

References

[1] U. Siemann, “Solvent cast technology - A versatile tool for thin film production,” *Prog. Colloid Polym. Sci.*, vol. 130, no. June, pp. 1–14, 2005.

[2] A. Karimi and W. M. A. Wan Daud, “Materials, preparation, and characterization of PVA/MMT nanocomposite hydrogels: A review,” *Polym. Compos.*, p. n/a-n/a, Aug. 2015.

[3] V. Goodship and D. K. Jacobs, “Polyvinyl alcohol: materials, processing and applications,” 2009.

[4] N. Georgieva, R. Bryaskova, and R. Tzoneva, “New Polyvinyl alcohol-based hybrid materials for biomedical application,” 2012.

[5] J. Wang, X. Wang, C. Xu, M. Zhang, and X. Shang, “Preparation of graphene/poly(vinyl alcohol) nanocomposites with enhanced mechanical properties and water resistance,” *Polym. Int.*, vol. 60, no. 5, pp. 816–822, 2011.

[6] P. Structures, “Polymer Structures,” pp. 489–522, 1983.

[7] H. Gleiter, “Materials with ultrafine microstructures: Retrospectives and perspectives,” *Nanostructured Mater.*, vol. 1, no. 1, pp. 1–19, Jan. 1992.

[8] R. Surudžić, A. Janković, M. Mitrić, I. Matić, Z. D. Juranić, L. Živković, V. Mišković-

Stanković, K. Y. Rhee, S. J. Park, and D. Hui, “The effect of graphene loading on mechanical, thermal and biological properties of poly(vinyl alcohol)/graphene nanocomposites,” *J. Ind. Eng. Chem.*, vol. 34, pp. 250–257, 2016.

[9] J. Jose, S. K. De, M. A. A. Al Ma’adeed, J. Bhadra Dakua, P. A. Sreekumar, R. Sougrat, and M. A. Al-Harthi, “Compatibilizing role of carbon nanotubes in poly(vinyl alcohol)/starch blend,” *Starch/Staerke*, vol. 67, no. 1–2, pp. 147–153, 2015.

[10] P. A. Sreekumar, M. A. Al-Harthi, and S. K. De, “Effect of glycerol on thermal and mechanical properties of polyvinyl alcohol/starch blends,” *J. Appl. Polym. Sci.*, vol. 123, no. 1, pp. 135–142, Jan. 2012.

[11] J. Jose, F. Shehzad, and M. A. Al-Harthi, “Preparation method and physical, mechanical, thermal characterization of poly(vinyl alcohol)/poly(acrylic acid) blends,” *Polym. Bull.*, vol. 71, no. 11, pp. 2787–2802, 2014.

[12] M. Zubair, J. Jose, A. H. Emwas, and M. A. Al-Harthi, “Effect of modified graphene and microwave irradiation on the mechanical and thermal properties of poly(styrene-co-methyl methacrylate)/graphene nanocomposites,” *Surf. Interface Anal.*, vol. 46, no. 9, pp. 630–639, 2014.

[13] K. K. Sadasivuni, D. Ponnamma, J. Kim, and S. Thomas, “Graphene-based polymer nanocomposites in electronics,” *Graphene-Based Polym. Nanocomposites Electron.*, pp. 1–382, 2015.

[14] K. S. Novoselov, a K. Geim, S. V Morozov, D. Jiang, Y. Zhang, S. V Dubonos, I. V Grigorieva, and a a Firsov, "Electric field effect in atomically thin carbon films.," *Science (80-.).*, vol. 306, no. 5696, pp. 666–9, Oct. 2004.

[15] V. Dhand, K. Y. Rhee, H. J. Kim, and D. H. Jung, "A Comprehensive Review of Graphene Nanocomposites : Research Status and Trends," vol. 2013, 2017.

[16] S. Park and R. S. Ruoff, "Chemical methods for the production of graphenes," *Nat. Nanotechnol.*, vol. 4, no. 4, pp. 217–224, Apr. 2009.

[17] D. Li, M. B. Müller, S. Gilje, R. B. Kaner, and G. G. Wallace, "Processable aqueous dispersions of graphene nanosheets," *Nat. Nanotechnol.*, vol. 3, no. 2, pp. 101–105, Feb. 2008.

[18] A. K. Geim, "Graphene: status and prospects.," *Science*, vol. 324, no. 5934, pp. 1530–4, Jun. 2009.

[19] J. Guo, L. Ren, R. Wang, C. Zhang, Y. Yang, and T. Liu, "Water dispersible graphene noncovalently functionalized with tryptophan and its poly(vinyl alcohol) nanocomposite," *Compos. Part B Eng.*, vol. 42, no. 8, pp. 2130–2135, 2011.

[20] G. W. Jeon, J.-E. An, and Y. G. Jeong, "High performance cellulose acetate propionate composites reinforced with exfoliated graphene," *Compos. Part B Eng.*, vol. 43, no. 8, pp. 3412–3418, 2012.

[21] J. Jose, M. A. Al-Harthi, M. A. A. AlMa'adeed, J. B. Dakua, and S. K. De, "Effect of graphene loading on thermomechanical properties of poly(vinyl alcohol)/starch blend," *J. Appl. Polym. Sci.*, vol. 132, no. 16, pp. 1–8, 2015.

[22] "Thermal Properties of Polymer Nanocomposites," 2012.

[23] J. K. Hobbs and J. K. Hobbs, "Crystallization Kinetics," in *Encyclopedia of Polymer Science and Technology*, Hoboken, NJ, USA: John Wiley & Sons, Inc., 2004.

[24] E. Piorkowska, A. Galeski, and J.-M. Haudin, "Critical assessment of overall crystallization kinetics theories and predictions," *Prog. Polym. Sci.*, vol. 31, no. 6, pp. 549–575, 2006.

[25] L. Mandelkern, F. A. Quinn, and P. J. Flory, "Crystallization Kinetics in High Polymers. I. Bulk Polymers," *J. Appl. Phys.*, vol. 25, no. 7, p. 830, 1954.

[26] A. T. Lorenzo, M. L. Arnal, J. Albuerne, and A. J. M??ller, "DSC isothermal polymer crystallization kinetics measurements and the use of the Avrami equation to fit the data: Guidelines to avoid common problems," *Polym. Test.*, vol. 26, no. 2, pp. 222–231, 2007.

[27] M. Avrami, "Kinetics of Phase Change. I General Theory," *J. Chem. Phys.*, vol. 7, no. 12, p. 1103, 1939.

[28] Z. Dobkowski, "Thermal analysis techniques for characterization of polymer materials,"

Polym. Degrad. Stab., vol. 91, no. 3, pp. 488–493, 2006.

[29] P. Paik and K. K. Kar, "Kinetics of thermal degradation and estimation of lifetime for polypropylene particles: Effects of particle size," *Polym. Degrad. Stab.*, vol. 93, no. 1, pp. 24–35, 2008.

[30] S. Vyazovkin, I. Dranca, X. Fan, and R. Advincula, "Degradation and Relaxation Kinetics of Polystyrene−Clay Nanocomposite Prepared by Surface Initiated Polymerization," *J. Phys. Chem. B*, vol. 108, no. 31, pp. 11672–11679, Aug. 2004.

[31] A. Khawam and D. R. Flanagan, "Solid-State Kinetic Models: Basics and Mathematical Fundamentals," *J. Phys. Chem. B*, vol. 110, no. 35, pp. 17315–17328, Sep. 2006.

[32] N. Koga and H. Tanaka, "A physico-geometric approach to the kinetics of solid-state reactions as exemplified by the thermal dehydration and decomposition of inorganic solids," *Thermochim. Acta*, vol. 388, no. 1, pp. 41–61, 2002.

[33] A. Habibi, "Kinetic modeling of the thermal degradation of methacrylate copolymers by thermogravimetric methods," *Int. J. Chem. React. Eng.*, 2007.

[34] V. Mamleev, S. Bourbigot, M. Le Bras, J. Yvon, and J. Lefebvre, "Model-free method for evaluation of activation energies in modulated thermogravimetry and analysis of cellulose decomposition," *Chem. Eng. Sci.*, vol. 61, no. 4, pp. 1276–1292, 2006.

[35] X. Sheng, M. Akinc, and M. R. Kessler, “Cure kinetics of thermosetting bisphenol E cyanate ester,” *J. Therm. Anal. Calorim.*, vol. 93, no. 1, pp. 77–85, Jul. 2008.

[36] R. Zong, Y. Hu, N. Liu, S. Wang, and G. Liao, “Evaluation of the thermal degradation of PC/ABS/montmorillonite nanocomposites,” *Polym. Adv. Technol*, vol. 16, pp. 725–731, 2005.

[37] S. Wen and D. D. L. Chung, “Pitch-matrix composites for electrical, electromagnetic and strain-sensing applications,” *J. Mater. Sci.*, vol. 40, no. 15, pp. 3897–3903, Aug. 2005.

[38] N. C. Das and S. Maiti, “Electromagnetic interference shielding of carbon nanotube/ethylene vinyl acetate composites,” *J. Mater. Sci.*, vol. 43, no. 6, pp. 1920–1925, Mar. 2008.

[39] J. Liang, Y. Wang, Y. Huang, Y. Ma, Z. Liu, J. Cai, C. Zhang, H. Gao, and Y. Chen, “Electromagnetic interference shielding of graphene/epoxy composites,” *Carbon N. Y.*, vol. 47, no. 3, pp. 922–925, 2009.

[40] M. B. Bryning, M. F. Islam, J. M. Kikkawa, and A. G. Yodh, “Very low conductivity threshold in bulk isotropic single-walled carbon nanotube-epoxy composites,” *Adv. Mater.*, vol. 17, no. 9, pp. 1186–1191, 2005.

[41] A. Boudenne, L. Ibos, E. Géhin, M. Fois, and J. C. Majesté, “Anomalous behavior of thermal conductivity and diffusivity in polymeric materials filled with metallic particles,”

vol. 40, pp. 4163–4167, 2005.

[42] S. Shang, L. Li, X. Yang, and Y. Wei, “Polymethylmethacrylate-carbon nanotubes composites prepared by microemulsion polymerization for gas sensor,” *Compos. Sci. Technol.*, vol. 69, no. 7, pp. 1156–1159, 2009.

[43] M. Rahaman, T. K. Chaki, and D. Khastgir, “Temperature Dependent Electrical Properties of Conductive Composites (Behavior at Cryogenic Temperature and High Temperatures),” *Adv. Mater. Res.*, vol. 123–125, pp. 447–450, Aug. 2010.

[44] L. M. Clayton, B. Knudsen, M. Cinke, M. Meyyappan, and J. P. Harmon, “DC conductivity and interfacial polarization in PMMA/nanotube and PMMA/soot composites.,” *J. Nanosci. Nanotechnol.*, vol. 7, no. 10, pp. 3572–9, Oct. 2007.

[45] M. B. H. Othman, M. R. Ramli, L. Y. Tyng, Z. Ahmad, and H. M. Akil, “Dielectric constant and refractive index of poly (siloxane-imide) block copolymer,” *Mater. Des.*, vol. 32, no. 6, pp. 3173–3182, 2011.

[46] M. Rahaman, T. K. Chaki, and D. Khastgir, “Modeling of DC conductivity for ethylene vinyl acetate (EVA)/polyaniline conductive composites prepared through insitu polymerization of aniline in EVA matrix,” *Compos. Sci. Technol.*, vol. 72, no. 13, pp. 1575–1580, 2012.

[47] D. Khastgir, H. . Maiti, and P. . Bandyopadhyay, “Polystyrene-titania composite as a

dielectric material," *Mater. Sci. Eng.*, vol. 100, pp. 245–253, Apr. 1988.

[48] S. Ibrahim and A. S. Ayesh, "Electrical and optical properties of functionalized multiwalled carbon nanotubes/poly (3-octylthiophene)/polystyrene composites," *J. Thermoplast. Compos. Mater.*, p. 0892705713480517-, 2013.

[49] C. C. Wu, Y. C. Chen, C. F. Yang, C. C. Su, and C. C. Diao, "The dielectric properties of epoxy/AlN composites," *J. Eur. Ceram. Soc.*, vol. 27, no. 13–15, pp. 3839–3842, 2007.

[50] a. S. Ayesh, S. S. Ibrahim, and a. a. Aljaafari, "Electrical, optical, and rheological properties of ozone-treated multiwalled carbon nanotubes-polystyrene nanocomposites," *J. Reinf. Plast. Compos.*, vol. 32, no. 6, pp. 359–370, 2012.

[51] J.-H. Lin, Z.-I. Lin, Y.-J. Pan, C.-K. Chen, C.-L. Huang, C.-H. Huang, and C.-W. Lou, "Improvement in Mechanical Properties and Electromagnetic Interference Shielding Effectiveness of PVA-Based Composites: Synergistic Effect Between Graphene Nano-Sheets and Multi-Walled Carbon Nanotubes," *Macromol. Mater. Eng.*, vol. 301, no. 2, pp. 199–211, Feb. 2016.

[52] K. Fujimori, M. Gopiraman, H.-K. Kim, B.-S. Kim, and I.-S. Kim, "Mechanical and electromagnetic interference shielding Properties of poly(vinyl alcohol)/graphene and poly(vinyl alcohol)/multi-walled carbon nanotube composite nanofiber mats and the effect of Cu top-layer coating.," *J. Nanosci. Nanotechnol.*, vol. 13, no. 3, pp. 1759–64, Mar. 2013.

[53] R. L. Mccullough, “Generalized Combining Rules for Predicting Transport Properties of Composite Materials Fi = ~ ’ KijG j,” vol. 22, 1985.

[54] S. D. Cho, S. Y. Lee, J. G. Hyun, and K. W. Paik, “Comparison of theoretical predictions and experimental values of the dielectric constant of epoxy/BaTiO3 composite embedded capacitor films,” *J. Mater. Sci. Mater. Electron.*, vol. 16, no. 2, pp. 77–84, 2005.

[55] F. Bueche, “Electrical resistivity of conducting particles in an insulating matrix,” *J. Appl. Phys.*, vol. 43, no. 11, pp. 4837–4838, 1972.

[56] H. T. Vo and F. G. Shi, “Towards model-based engineering of optoelectronic packaging materials: Dielectric constant modeling,” *Microelectronics J.*, vol. 33, no. 5–6, pp. 409–415, 2002.

[57] N. Jayasundere and B. V. Smith, “Dielectric constant for binary piezoelectric 0-3 composites,” *J. Appl. Phys.*, vol. 73, no. 5, pp. 2462–2466, 1993.

[58] B. Lestriez, A. Maazouz, J. . Gerard, H. Sautereau, G. Boiteux, G. Seytre, and D. E. Kranbuehl, “Is the Maxwell–Sillars–Wagner model reliable for describing the dielectric properties of a core–shell particle–epoxy system?,” *Polymer (Guildf).*, vol. 39, no. 26, pp. 6733–6742, 1998.

[59] R. M. Scarisbrick, B. G. and G. F. G, B. L. K. H. and van P. B. I. C. F, B. J. D, B. F. P. and T. D, B. D. A. G, B. D, C. J. W, F. P. J, F. A. R, F. E. O, F. R, G. J. H. and di M. E.

A, G. J. H. and di M. E. A, G. R. B. and T. T. Y, G. B. and F. R. M, M. A. and T. D. T, M. J. C, M. R. E. and T. C. W, M. R. C. and W. P. C, M. A. A. and L. C. S, N. R. H, P. M. H. and B. B. B. S. T, S. A, S. M. L, S. M. L, van L. P. R, and W. W. N. (Jr) and C. F. R. Voet A, "Electrically conducting mixtures," *J. Phys. D. Appl. Phys.*, vol. 6, no. 17, p. 316, Nov. 1973.

[60] L. Feng, W. Li, J. Ren, and X. Qu, "Electrochemically and DNA-triggered cell release from ferrocene/β-cyclodextrin and aptamer modified dualfunctionalized graphene substrate," *Nano Res.*, vol. 8, no. 3, pp. 887–899, Mar. 2015.

[61] D. Banerjee, A. Jha, and K. K. Chattopadhyay, "Synthesis and characterization of water soluble functionalized amorphous carbon nanotube-poly(vinyl alcohol) composite," *Macromol. Res.*, vol. 20, no. 10, pp. 1021–1028, Oct. 2012.

[62] G. Wu, Y. Tang, and R. Weng, "Dispersion of nano-carbon filled polyimide composites using self-degradated low molecular poly(amic acid) as impurity-free dispersant," *Polym. Degrad. Stab.*, vol. 95, no. 9, pp. 1449–1455, 2010.

[63] D. McIntosh, V. N. Khabashesku, and E. V. Barrera, "Benzoyl Peroxide Initiated In Situ Functionalization, Processing, and Mechanical Properties of Single-Walled Carbon Nanotube−Polypropylene Composite Fibers," *J. Phys. Chem. C*, vol. 111, no. 4, pp. 1592–1600, Feb. 2007.

[64] a a Miller, "EFFECTS OF HIGH-ENERGY RADIATION ON POLYMERS A. A.

Miller," no. 1, pp. 774–781.

[65] S. Raghu, S. Kilarkaje, G. Sanjeev, G. K. Nagaraja, and H. Devendrappa, "Effect of electron beam irradiation on polymer electrolytes: Change in morphology, crystallinity, dielectric constant and AC conductivity with dose," *Radiat. Phys. Chem.*, vol. 98, pp. 124–131, 2014.

[66] S. J. Zhang and H. Q. Yu, "Radiation-induced degradation of polyvinyl alcohol in aqueous solutions," *Water Res.*, vol. 38, no. 2, pp. 309–316, 2004.

[67] H. L. Chia, J. Jacob, and F. Y. C. Boey, "The microwave radiation effect on the polymerization of styrene," *J. Polym. Sci. Part A Polym. Chem.*, vol. 34, no. 11, pp. 2087–2094, 1996.

[68] M. Zubair, F. Shehzad, and M. A. Al-harthi, "Thermochimica Acta Impact of modified graphene and microwave irradiation on thermal stability and degradation mechanism of poly (styrene- co -methyl meth acrylate)," *Thermochim. Acta*, vol. 633, pp. 48–55, 2016.

[69] D. F. Stein, *Microwave Processing of Materials*. 1994.

[70] M. A. Al-Harthi, "Influence of applying microwave radiation on the LDPE/MWCNTs nanocomposite," *Polym. Compos.*, vol. 35, no. 10, pp. 2036–2042, Oct. 2014.

[71] M. Zubair, J. Jose, and M. A. Al-Harthi, "Evaluation of mechanical and thermal properties

of microwave irradiated poly (styrene-co-methyl methacrylate)/graphene nanocomposites," *Compos. Interfaces*, vol. 22, no. 7, pp. 595–610, Sep. 2015.

[72] B. S. T.K., A. B. Nair, B. T. Abraham, P. M. S. Beegum, and E. T. Thachil, "Microwave exfoliated reduced graphene oxide epoxy nanocomposites for high performance applications," *Polymer (Guildf).*, vol. 55, no. 16, pp. 3614–3627, 2014.

[73] P. Sreekumar, M. a. Al-Harthi, and S. De, "Reinforcement of starch/polyvinyl alcohol blend using nano-titanium dioxide," *J. Compos. Mater.*, vol. 46, no. 25, pp. 3181–3187, 2012.

[74] S. P. Appu, S. K. De, M. J. Khan, and M. A. Al-Harthi, "Natural weather ageing of starch/polyvinyl alcohol blend: Effect of glycerol content," *J. Polym. Eng.*, vol. 33, no. 3, pp. 257–263, 2013.

[75] P. A. Sreekumar, M. A. Al-Harthi, and S. K. De, "Studies on compatibility of biodegradable starch/polyvinyl alcohol blends," *Polym. Eng. Sci.*, vol. 52, no. 10, pp. 2167–2172, Oct. 2012.

[76] P. A. Sreekumar, M. A. Al-Harthi, M. A. Gondal, and S. K. De, "Heterogeneity of laser-irradiated films of polyvinyl alcohol/starch blends: effect of glycerol content," *Surf. Interface Anal.*, vol. 45, no. 6, pp. 1047–1051, 2013.

[77] L. Deng, R. J. Young, R. Sun, G. Zhang, D. D. Lu, H. Li, and S. J. Eichhorn, "Unique

identification of single-walled carbon nanotubes in electrospun fibers," *J. Phys. Chem. C*, vol. 118, no. 41, pp. 24025–24033, 2014.

[78] Z. Li, R. J. Young, and I. a Kinloch, "Interfacial stress transfer in graphene oxide nanocomposites.," *ACS Appl. Mater. Interfaces*, vol. 5, no. 2, pp. 456–63, 2013.

[79] L. Deng, S. J. Eichhorn, C.-C. Kao, and R. J. Young, "The effective Young's modulus of carbon nanotubes in composites.," *ACS Appl. Mater. Interfaces*, vol. 3, no. 2, pp. 433–440, 2011.

[80] F. M. Blighe, K. Young, J. J. Vilatela, A. H. Windle, I. A. Kinloch, L. Deng, R. J. Young, and J. N. Coleman, "The effect of nanotube content and orientation on the mechanical properties of polymer-nanotube composite fibers: Separating intrinsic reinforcement from orientational effects," *Adv. Funct. Mater.*, vol. 21, no. 2, pp. 364–371, 2011.

[81] M. Lucas and R. J. Young, "Unique identification of single-walled carbon nanotubes in composites," *Compos. Sci. Technol.*, vol. 67, no. 10, pp. 2135–2149, 2007.

[82] P. Kannan, S. J. Eichhorn, and R. J. Young, "Deformation of isolated single-wall carbon nanotubes in electrospun polymer nanofibres," *Nanotechnology*, vol. 18, no. 23, p. 235707, 2007.

[83] J. Liang, Y. Huang, L. Zhang, Y. Wang, Y. Ma, T. Cuo, and Y. Chen, "Molecular-level dispersion of graphene into poly(vinyl alcohol) and effective reinforcement of their

nanocomposites," *Adv. Funct. Mater.*, vol. 19, no. 14, pp. 2297–2302, 2009.

[84] H. Kim, A. A. Abdala, and C. W. MacOsko, "Graphene/polymer nanocomposites," *Macromolecules*, vol. 43, no. 16, pp. 6515–6530, 2010.

[85] C. Gómez-Navarro, J. C. Meyer, R. S. Sundaram, A. Chuvilin, S. Kurasch, M. Burghard, K. Kern, and U. Kaiser, "Atomic structure of reduced graphene oxide," *Nano Lett.*, vol. 10, no. 4, pp. 1144–1148, 2010.

[86] J. T. Robinson, F. K. Perkins, E. S. Snow, Z. Wei, and P. E. Sheehan, "Reduced graphene oxide molecular sensors," *Nano Lett.*, vol. 8, no. 10, pp. 3137–3140, 2008.

[87] Y. Zhu, S. Murali, W. Cai, X. Li, J. W. Suk, J. R. Potts, and R. S. Ruoff, "Graphene and graphene oxide: Synthesis, properties, and applications," *Adv. Mater.*, vol. 22, no. 35, pp. 3906–3924, 2010.

[88] W. S. Hummers and R. E. Offeman, "Preparation of Graphitic Oxide," *J. Am. Chem. Soc.*, vol. 80, no. 6, pp. 1339–1339, Mar. 1958.

[89] Y. Xu, W. Hong, H. Bai, C. Li, and G. Shi, "Strong and ductile poly(vinyl alcohol)/graphene oxide composite films with a layered structure," *Carbon N. Y.*, vol. 47, no. 15, pp. 3538–3543, Dec. 2009.

[90] X. Zhao, Q. Zhang, D. Chen, and P. Lu, "Enhanced Mechanical Properties of Graphene-

Based Poly(vinyl alcohol) Composites," *Macromolecules*, vol. 43, no. 5, pp. 2357–2363, Mar. 2010.

[91] L. Zhang, Z. Wang, C. Xu, Y. Li, J. Gao, W. Wang, and Y. Liu, "High strength graphene oxide/polyvinyl alcohol composite hydrogels," *J. Mater. Chem.*, vol. 21, no. 28, p. 10399, 2011.

[92] H.-D. Huang, P.-G. Ren, J. Chen, W.-Q. Zhang, X. Ji, and Z.-M. Li, "High barrier graphene oxide nanosheet/poly(vinyl alcohol) nanocomposite films," *J. Memb. Sci.*, vol. 409, no. 410, pp. 156–163, Aug. 2012.

[93] H. K. F. Cheng, N. G. Sahoo, Y. P. Tan, Y. Pan, H. Bao, L. Li, S. H. Chan, and J. Zhao, "Poly(vinyl alcohol) nanocomposites filled with poly(vinyl alcohol)-grafted graphene oxide," *ACS Appl. Mater. Interfaces*, vol. 4, no. 5, pp. 2387–2394, 2012.

[94] C. Wang, Y. Li, G. Ding, X. Xie, and M. Jiang, "Preparation and characterization of graphene oxide/poly(vinyl alcohol) composite nanofibers via electrospinning," *J. Appl. Polym. Sci.*, vol. 127, no. 4, pp. 3026–3032, 2013.

[95] S. Lee, J.-Y. Hong, and J. Jang, "The effect of graphene nanofiller on the crystallization behavior and mechanical properties of poly(vinyl alcohol)," *Polym. Int.*, vol. 62, no. 6, pp. 901–908, 2013.

[96] I. a Latif, S. M. Abbas, and M. a Kadhum, "Hydrogen Bonds Effects on the Electrical

Properties of Pectin / Pva Graphene Nanocomposites," *Chem. Mater. Res.*, vol. 3, no. 1, pp. 1–12, 2013.

[97] Y. S. Ye, M. Y. Cheng, X. L. Xie, J. Rick, Y. J. Huang, F. C. Chang, and B. J. Hwang, "Alkali doped polyvinyl alcohol/graphene electrolyte for direct methanol alkaline fuel cells," *J. Power Sources*, vol. 239, pp. 424–432, 2013.

[98] H.-L. Ma, Y. Zhang, Q.-H. Hu, S. He, X. Li, M. Zhai, and Z.-Z. Yu, "Enhanced mechanical properties of poly(vinyl alcohol) nanocomposites with glucose-reduced graphene oxide," *Mater. Lett.*, vol. 102–103, pp. 15–18, 2013.

[99] S. Shang, L. Gan, C. W. M. Yuen, S. Jiang, and N. M. Luo, "The synthesis of graphene nanoribbon and its reinforcing effect on poly (vinyl alcohol)," *Compos. Part A Appl. Sci. Manuf.*, vol. 68, pp. 149–154, 2015.

[100] H. Somashekarappa, Y. Prakash, T. Demappa, and R. Somashekar, "Effect of microwave radiation on hydroxy propyl methyl cellulose polymer films and HPMC/poly(vinylpyrrolidone) polymer blend films using the wide-angle X-ray technique," *Radiat. Eff. Defects Solids*, vol. 168, no. 11–12, pp. 912–923, 2013.

[101] D. a. Gorin, D. G. Shchukin, a. I. Mikhailov, K. Köhler, S. a. Sergeev, S. a. Portnov, I. V. Taranov, V. V. Kislov, and G. B. Sukhorukov, "Effect of microwave radiation on polymer microcapsules containing inorganic nanoparticles," *Tech. Phys. Lett.*, vol. 32, no. 1, pp. 70–72, 2006.

[102] K. Venkatasubrahmanayam, B. Ram Babu, B. Poornaiah, and Y. Srinivasa Rao, “The effect of microwave radiation on polyvinyl chloride-graphite thick film resistors,” *Microelectron. Int.*, vol. 31, no. 2, pp. 99–103, 2014.

[103] C. Tsai, B. Rubin, E. Tatartschuk, J. R. Owens, I. Luzinov, and K. G. Kornev, “Efficiency of Microwave Heating of Weakly Loaded Polymeric Nanocomposites.”

[104] C. Products, T. Dow, and C. Company, “Changes in the crystalline c o n t e n t of irradiated linear polyethylenes upon ageing S. K. Bhateja 354,” vol. 23, pp. 654–655, 1982.

[105] C. Yeh, C. Chen, Y. Li, M. Cheng, and H. Chang, “f o o r y p o c y,” vol. 30, no. 5, 2011.

[106] F. Shehzad, M. Daud, and M. A. Al-Harthi, “Synthesis, characterization and crystallization kinetics of nanocomposites prepared by in situ polymerization of ethylene and graphene,” *J. Therm. Anal. Calorim.*, 2015.

[107] R. L. Blaine, N. Castle, B. Wunderlich, A. Press, and W. Conshohocken, “THERMAL APPLICATIONS NOTE Polymer Heats of Fusion,” *Society*, pp. 1–2.

[108] G. Z. Papageorgiou, A. Palani, D. Gilliopoulos, K. S. Triantafyllidis, and D. N. Bikiaris, “Mechanical properties and crystallization of high-density polyethylene composites with mesostructured cellular silica foam,” *J. Therm. Anal. Calorim.*, vol. 113, no. 3, pp. 1651–1665, Sep. 2013.

[109] B. A. Abdul-majeed, H. K. Hussain, and N. A. K. Al-sultanee, “Effect of Annealing on the Crystallization of Poly Vinyl Chloride for Drug Delivery System,” vol. 13, no. 2, pp. 29–36, 2012.

[110] S. P. Pawar, S. Stephen, S. Bose, and V. Mittal, “Tailored electrical conductivity, electromagnetic shielding and thermal transport in polymeric blends with graphene sheets decorated with nickel nanoparticles.,” *Phys. Chem. Chem. Phys.*, pp. 14922–14930, 2015.

[111] N. Ahad, E. Saion, and E. Gharibshahi, “Structural, thermal, and electrical properties of Pva-sodium salicylate solid composite polymer electrolyte,” *J. Nanomater.*, vol. 2012, 2012.

[112] S. Mahendia, Heena, G. Kandhol, U. P. Deshpande, and S. Kumar, “Determination of glass transition temperature of reduced graphene oxide-poly(vinyl alcohol) composites using temperature dependent Fourier transform infrared spectroscopy,” *J. Mol. Struct.*, vol. 1111, pp. 46–54, 2016.

[113] N. V. Medhekar, A. Ramasubramaniam, R. S. Ruoff, and V. B. Shenoy, “Hydrogen Bond Networks in Graphene Oxide Composite Paper: Structure and Mechanical Properties,” *ACS Nano*, vol. 4, no. 4, pp. 2300–2306, Apr. 2010.

[114] A. M. A. Ghaffar, “γ -Irradiation Effect on the Non-Crosslinked and Crosslinked Poly (vinyl alcohol) Films Experimental Materials Preparation of Poly (vinyl alcohol) Film Irradiation of Poly (vinyl alcohol) Film Fourier Transform Infrared (FTIR) Ultraviolet

Spectrop."

[115] L. Gongxu, C. Hongying, and L. Dongyuan, "The degradation in solid state of polyvinyl alcohol by gamma-irradiation," *Radiat. Phys. Chem.*, vol. 42, no. 1–3, pp. 229–232, Jul. 1993.

[116] N. V. Bhat, M. M. Nate, M. B. Kurup, V. A. Bambole, and S. Sabharwal, "Effect of γ-radiation on the structure and morphology of polyvinyl alcohol films," *Nucl. Instruments Methods Phys. Res. Sect. B Beam Interact. with Mater. Atoms*, vol. 237, no. 3–4, pp. 585–592, Aug. 2005.

[117] A. C. Ferrari and J. Robertson, "Resonant Raman spectroscopy of disordered, amorphous, and diamondlike carbon," *Phys. Rev. B*, vol. 64, no. 7, p. 75414, 2001.

[118] M. S. Dresselhaus, G. Dresselhaus, and R. Saito, "Physics of carbon nanotubes," *Carbon N. Y.*, vol. 33, no. 7, pp. 883–891, 1995.

[119] S. Stankovich, D. A. Dikin, R. D. Piner, K. A. Kohlhaas, A. Kleinhammes, Y. Jia, Y. Wu, S. T. Nguyen, and R. S. Ruoff, "Synthesis of graphene-based nanosheets via chemical reduction of exfoliated graphite oxide," *Carbon N. Y.*, vol. 45, no. 7, pp. 1558–1565, 2007.

[120] E. A. Bursali, S. Coskun, M. Kizil, and M. Yurdakoc, "Synthesis, characterization and in vitro antimicrobial activities of boron/starch/polyvinyl alcohol hydrogels," *Carbohydr.*

Polym., vol. 83, no. 3, pp. 1377–1383, 2011.

[121] S. K. Sharma, J. Prakash, and P. K. Pujari, "Effects of the molecular level dispersion of graphene oxide on the free volume characteristics of poly(vinyl alcohol) and its impact on the thermal and mechanical properties of their nanocomposites," *Phys. Chem. Chem. Phys.*, vol. 17, no. 43, pp. 29201–29209, 2015.

[122] N. Thayumanavan, P. Tambe, and G. Joshi, "Effect of Surfactant and Sodium Alginate Modification of Graphene on the Mechanical and Thermal Properties of Polyvinyl Alcohol (Pva) Nanocomposites," *Cellul. Chem. Technol. Cellul. Chem. Technol*, vol. 49, no. 1, pp. 69–80, 2015.

[123] V. M. Aslanian, V. I. Vardanian, M. H. Avetisian, S. S. Felekian, and S. R. Ayvasian, "Effect of radiation on the crystallinity of low-density polyethylene," vol. 28, pp. 755–757, 1987.

[124] A. Torikai, R. Geetha, S. Nagaya, and K. Fueki, "Radiation-induced degradation of polyethylene: Role of amorphous region in the formation of oxygenated products and the mechanical properties," *Polym. Degrad. Stab.*, vol. 16, no. 2, pp. 199–212, Jan. 1986.

[125] S. Mishra, R. Bajpai, R. Katare, and A. K. Bajpai, "Radiation induced crosslinking effect on semiinterpenetrating polymer networks of poly(vinyl alcohol)," *Express Polym. Lett.*, vol. 1, no. 7, pp. 407–415, 2007.

[126] S. Lee, J.-Y. Hong, and J. Jang, “The effect of graphene nanofiller on the crystallization behavior and mechanical properties of poly(vinyl alcohol),” *Polym. Int.*, vol. 62, no. 6, pp. 901–908, Jun. 2013.

[127] E. Oral, C. Godleski-Beckos, B. W. Ghali, A. J. Lozynsky, and O. K. Muratoglu, “Effect of cross-link density on the high pressure crystallization of UHMWPE.,” *J. Biomed. Mater. Res. B. Appl. Biomater.*, vol. 90, no. 2, pp. 720–9, Aug. 2009.

[128] G. S. Trick, “The crystallization of modified cis-polybutadiene,” *J. Polym. Sci.*, vol. 41, no. 138, pp. 213–217, Dec. 1959.

[129] A. L. Saroj, S. K. Chaurasia, S. Kataria, and R. K. Singh, “Isothermal and non-isothermal crystallization kinetics of PVA + ionic liquid [BDMIM][BF_4]-based polymeric films,” *Phase Transitions*, pp. 1–20, Oct. 2015.

[130] M. Trujillo, M. L. Arnal, A. J. Müller, E. Laredo, S. Bredeau, D. Bonduel, and P. Dubois, “Thermal and Morphological Characterization of Nanocomposites Prepared by in-Situ Polymerization of High-Density Polyethylene on Carbon Nanotubes,” *Macromolecules*, vol. 40, no. 17, pp. 6268–6276, Aug. 2007.

[131] B. Fillon, B. Lotz, A. Thierry, and J. C. Wittmann, “Self-nucleation and enhanced nucleation of polymers. Definition of a convenient calorimetric ‘efficiency scale’ and evaluation of nucleating additives in isotactic polypropylene (α phase),” *J. Polym. Sci. Part B Polym. Phys.*, vol. 31, no. 10, pp. 1395–1405, Sep. 1993.

[132] B. Fillon, J. C. Wittmann, B. Lotz, and A. Thierry, “Self-nucleation and recrystallization of isotactic polypropylene (α phase) investigated by differential scanning calorimetry,” *J. Polym. Sci. Part B Polym. Phys.*, vol. 31, no. 10, pp. 1383–1393, Sep. 1993.

[133] S. Xin, Y. Li, H. Zhao, Y. Bian, W. Li, C. Han, Q. Dong, Z. Ning, and L. Dong, “Confinement crystallization of poly(l-lactide) induced by multiwalled carbon nanotubes and graphene nanosheets,” *J. Therm. Anal. Calorim.*, vol. 122, no. 1, pp. 379–391, Oct. 2015.

[134] J. W. Gilman, D. L. VanderHart, and T. Kashiwagi, “Thermal Decomposition Chemistry of Poly (vinyl alcohol),” *Fire Polym. II*, vol. 6, no. 2, pp. 415–424, 1995.

[135] H. Yang, S. Xu, L. Jiang, and Y. Dan, “Thermal Decomposition Behavior of Poly (Vinyl Alcohol) with Different Hydroxyl Content Thermal Decomposition Behavior of Poly (Vinyl Alcohol) with Different Hydroxyl Content,” vol. 2348, no. May, 2016.

[136] B. J. Holland and J. N. Hay, “The thermal degradation of poly (vinyl alcohol),” vol. 42, pp. 6775–6783, 2001.

[137] F. Barroso-bujans, J. A. Pomposo, and J. Colmenero, “Thermal Stability of Polymers Con fi ned in Graphite Oxide,” 2013.

[138] W. Gao, L. B. Alemany, L. Ci, and P. M. Ajayan, “New insights into the structure and reduction of graphite oxide.,” *Nat. Chem.*, vol. 1, no. 5, pp. 403–8, Aug. 2009.

[139] A. Lerf, H. He, M. Forster, and J. Klinowski, “Structure of Graphite Oxide Revisited ‖,” *J. Phys. Chem. B*, vol. 102, no. 23, pp. 4477–4482, Jun. 1998.

[140] P. S. Thomas, J. Guerbois, G. F. Russell, and B. J. Briscoe, “FTIR STUDY OF THE THERMAL DEGRADATION OF POLY (VINYL ALCOHOL),” vol. 64, no. 2001, pp. 501–508, 2007.

[141] A. Olad, “7 Polymer/Clay Nanocomposites.”

[142] D. R. Paul and L. M. Robeson, “Polymer nanotechnology: Nanocomposites,” *Polymer (Guildf).*, vol. 49, no. 15, pp. 3187–3204, 2008.

[143] T.-T. Su, H. Jiang, and H. Gong, “Thermal Stabilities and the Thermal Degradation Kinetics of Poly(ε-Caprolactone),” *Polym. Plast. Technol. Eng.*, vol. 47, no. 4, pp. 398–403, Mar. 2008.

[144] K. Chrissafis, “Kinetics of thermal degradation of polymers,” *J. Therm. Anal. Calorim.*, vol. 95, no. 1, pp. 273–283, Jan. 2009.

[145] W. Weng, G. Chen, D. Wu, X. Chen, J. Lu, and P. Wang, “Fabrication and characterization of nylon 6/foliated graphite electrically conducting nanocomposite,” *J. Polym. Sci. Part B Polym. Phys.*, vol. 42, no. 15, pp. 2844–2856, 2004.

[146] F. Bueche, “Electrical resistivity of conducting particles in an insulating matrix,” *J. Appl.*

Phys., vol. 43, no. 11, p. 4837, 1972.

[147] N. J. S. Sohi, M. Rahaman, and D. Khastgir, "Dielectric property and electromagnetic interference shielding effectiveness of ethylene vinyl acetate-based conductive composites: Effect of different type of carbon fillers," *Polym. Compos.*, vol. 32, no. 7, pp. 1148–1154, Jul. 2011.

[148] M. Chaharmahali, Y. Hamzeh, G. Ebrahimi, A. Ashori, and I. Ghasemi, "Effects of nano-graphene on the physico-mechanical properties of bagasse/polypropylene composites," *Polym. Bull.*, vol. 71, no. 2, pp. 337–349, Feb. 2014.

[149] X. Lu, R. Qian, and N. Brown, "The effect of crystallinity on fracture and yielding of polyethylenes," *Polymer (Guildf).*, vol. 36, no. 22, pp. 4239–4244, 1995.

[150] D. S. Li, H. Garmestani, R. G. Alamo, and S. R. Kalidindi, "The role of crystallinity in the crystallographic texture evolution of polyethylenes during tensile deformation," *Polymer (Guildf).*, vol. 44, no. 18, pp. 5355–5367, 2003.

[151] H. Liu and T. J. Webster, "Mechanical properties of dispersed ceramic nanoparticles in polymer composites for orthopedic applications.," *Int. J. Nanomedicine*, vol. 5, pp. 299–313, 2010.

Vitae

Name	:Hafiz Muhammad Afzal
Nationality	:Pakistani
Date of Birth	:11/19/1986
Email	:hafiz_afzal24@yahoo.com
Address	:House # 3, Milad street, Bhamman Jhugian, Bund road, Amir road, Shad bagh, Lahore, Pakistan.
Academic Background	:BSc Chemical Engineering, University of Punjab, Lahore, Pakistan.